Available online at www.sciencedirect.com
ScienceDirect
Comput. Methods Appl. Mech. Engrg. 196 (2007) 4027–4044
Computer methods in applied mechanics and engineering
www.elsevier.com/locate/cma

On deformational and configurational mechanics of micromorphic hyperelasticity – Theory and computation

C. Britta Hirschberger, Ellen Kuhl, Paul Steinmann *

Department of Mechanical Engineering, Chair of Applied Mechanics, University of Kaiserslautern, P.O. Box 3049, D-67653 Kaiserslautern, Germany

Received 6 June 2006; received in revised form 20 November 2006; accepted 26 February 2007
Available online 8 May 2007

Abstract

A micromorphic continuum formulation is presented in the context of both, the spatial- and the material-motion problem. For both approaches the kinematics as well as the balance relations together with the various representations of the occurring stress fields are derived. The relations between the spatial-motion problem and the material-motion problem quantities are examined in detail. Upon a hyperelastic constitutive assumption a finite-element approximation is derived and the material–force method, which is especially suited for defect-mechanics problems, is successfully applied to the present micromorphic continuum theory.

Keywords: Micromorphic continua; Configurational mechanics; Material forces; Finite element method

1. Introduction

The micromorphic continuum theory is used to describe materials which possess a significant microstructure and therefore exhibit scale-dependent behaviour. These microstructures are viewed as so-called microcontinua, which are assumed to be attached to each physical point and may experience both stretch and rotation deformations which are affine throughout the microcontinuum, nevertheless kinematically independent from the deformation on the macroscale.

The micromorphic continuum as a microcontinuum theory has first been introduced by Eringen [6,7] and is part of the group of so-called generalised continua for which the couple-stress theory of the brothers Cosserat and Cosserat [2] laid the foundation in the early 20th century. For related early developments the reader is referred to [31,32,22,13], just to mention a few. The so-called micropolar and microstretch continua may be considered as special cases of the micromorphic theory, since here specific constraints apply on the deformation of the microcontinuum. For instance in the case of the micropolar continuum, the microcontinuum may only experience rotation, see the contributions of [26,29,4] as well as those from the group of Tsakmakis (e.g., [9,3]), just to mention a few. A comprehensive overview on microcontinuum theories can be found in the contemporary monograph of Eringen [8]. Not only the different microcontinuum theories are congeneric, additionally, close relations between the latter and other nonlocal theories exist. Particularly the micromorphic and the second-order gradient theory can be transferred into each other by limit considerations, as has recently been shown by Kirchner and Steinmann [11]. This close relation allows to transfer the constitutive and finite-element formulations that were originally developed for micromorphic continua, to second-order gradient theories. As examples for such formulations of the gradient elasticity serve for instance the following contributions: Shu et al. [25] and Amanatidou and Aravas [1] for small deformations, as well as, extended to large deformations, Shu and Barlow [24] and – in the context of a homogenisation procedure [14–16].

* Corresponding author. Tel.: +49 631 205 2419; fax: +49 631 205 2128.
E-mail addresses: bhirsch@rhrk.uni-kl.de (C. Britta Hirschberger), ekuhl@rhrk.uni-kl.de (E. Kuhl), ps@rhrk.uni-kl.de (P. Steinmann).

0045-7825/$ - see front matter
doi:10.1016/j.cma.2007.02.015

Generally the deformation of continuum bodies can be described in two manners: One perspective is the so-called deformational mechanics and the other is the concept of configurational mechanics. Within deformational mechanics – or rather the *spatial-motion problem* – the spatial-motion of a physical point with particular material position is observed with the change of time – "*quo vadis*?". This description is characterised on the one hand by a parametrisation of the occurring quantities by the material position and on the other hand by the fact that these quantities belong to the spatial manifold (or are two-point tensors mapping towards the spatial manifold). Opposed to that, in the configurational-mechanics perspective, which we refer to as the *material-motion problem*, the spatial placement is fixed while the material origin of physical points passing by is the unknown quantity of observation – "*unde venis*?". The material-motion problem is formulated in material quantities (or two-point quantities mapping to the material manifold) which are parameterised by the spatial position.

In the spatial-motion problem we deal with the intuitively-known and widely-used spatial forces, which are defined as being energetically conjugate to variations in the spatial placement of physical points at fixed material position. Contrary to that, the perspective of the material-motion problem yields the so-called *material forces*. These are energetically conjugate to variations in the material position of a particular physical point. They are characterised in the literature to act as driving forces for the propagation of defects such as cracks and voids. Thus the material forces can for instance serve as criteria for crack propagation. For references on the concept of deformational vs. configurational mechanics in general and the material force method in particular, see for instance the contributions of Maugin and coworkers [5,19,20,23,21], Gurtin [10] or the group of Steinmann [27,28,30,17,18] as well as the references cite therein. It suggests itself to apply this dual perspective and within this context especially the material force method to the micromorphic continuum. From this, besides a deeper understanding of the theory, we strive for the predictive character of the material forces for fracture-mechanics considerations within the micromorphic continuum. Due to the relations shown in Kirchner and Steinmann [11], the full configurational-mechanics perspective on the second-order gradient theory given by [12], is especially helpful to establish the analogous perspective on the present micromorphic continuum.

Consequently, in this contribution a micromorphic continuum formulation is presented from the dual perspectives of both deformational and configurational mechanics. The kinematics is presented for finite deformations including the macro and the microcontributions. A restriction to isotropic hyperelasticity ensures the existence of a potential energy. For conservative static problems Dirichlet's principle results in the Euler–Lagrange equations, i.e., the balance of momentum in its strong form. Thus upon the definition of proper micromorphic kinematics, a variation of the potential energy renders the weak form of the balance of momentum together with Neumann boundary conditions, while the variations of primary kinematic variables have to satisfy the homogeneous Dirichlet boundary conditions. Based on the material-motion description, the material force method is applied, which, due to the existence of the microscale, bears the micromorphic material forces as well as additional higher-order quantities.

The article is structured as follows. In Section 2 the micromorphic continuum is introduced and its description is derived from a complete configurational-mechanics perspective. In Section 3 we establish a straightforward constitutive formulation which enables us to perform a finite-element approximation for the micromorphic continuum as presented in Section 4. Numerical examples incorporating parametric studies and the evaluation of the occurring material force quantities are computed in Section 5. The contribution closes with a short summary and a brief outlook on further research on the field.

2. The micromorphic continuum

As indicated before, the micromorphic continuum is described as a macrocontinuum of which each physical point is endowed with a microstructure referred to as the microcontinuum. These microcontinua may experience arbitrary deformations consisting of both stretch and rotation which are required to be affine, nevertheless kinematically independent from the macrocontinuum. A point $\mathscr{P}$ on the macroscale is described by the placement vectors $\boldsymbol{X}$ in the material configuration $\mathscr{B}_0$ and $\boldsymbol{x}$ in the spatial configuration $\mathscr{B}_t$. On the microscale, a point $\bar{\mathscr{P}}$ of the microcontinuum is denoted with the microplacement vectors $\bar{\boldsymbol{X}}$ in the material configuration $\bar{\mathscr{B}}_0$ and $\bar{\boldsymbol{x}}$ in the spatial configuration $\bar{\mathscr{B}}_t$, respectively.

Since a material point is equipped with a microstructure that is kinematically independent, additional balance equations besides the ordinary balance of momentum have to be considered for the micromorphic theory. These may be obtained by an energy consideration, which is here derived from Dirichlet's principle. Here the set of state variables is given by $\mathscr{S} = \{\boldsymbol{\varphi}, \bar{\boldsymbol{F}}\}$, wherein the first argument describes the macrostructural kinematics while the second characterises the deformation of the microcontinuum. A constitutive functional is to be found, which in the most general hyperelastic case incorporates the following dependencies: $\mathscr{C} = \mathscr{C}(\boldsymbol{\varphi}, \nabla_{\boldsymbol{X}}\boldsymbol{\varphi}, \bar{\boldsymbol{F}}, \nabla_{\boldsymbol{X}}\bar{\boldsymbol{F}};\ \boldsymbol{X})$.

First, the spatial-motion problem is presented in Section 2.1, before the material-motion problem described in Section 2.2. Both approaches are compared in Section 2.3. The following derivations of the spatial-motion problem follow the line of the finite-deformation part of Kirchner and Steinmann [11], while for the material-motion problem, parallels to the material settings of the second-order gradient theory as presented by Kirchner and Steinmann [12] can be recognised.

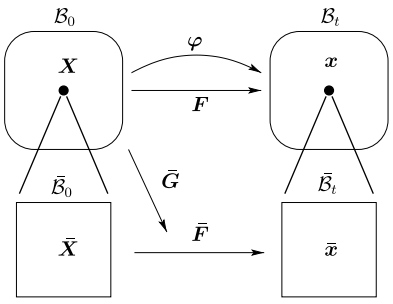

Fig. 1. Spatial-motion problem: micromorphic deformation maps.

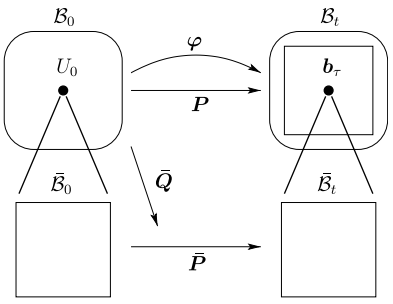

Fig. 2. Spatial-motion problem: Piola-type stress measures derived from hyperelasticity, $\tau = 0$, t.

2.1. Spatial-motion problem – quo vadis?

In the framework of the spatial-motion problem of the micromorphic continuum, first the kinematic relations are introduced. By the consideration of the stationarity of the potential energy at static equilibrium, the local balance of momentum with the corresponding boundary conditions is derived in a two-point formulation. In the sequel the description is transformed to a purely spatial formulation by push-forward operations on the quantities and operators.

2.1.1. Kinematic relations

Within the micromorphic continuum, the macro and the microcontinuum kinematics are considered as illustrated in Fig. 1. On the macroscale the spatial-motion deformation map is defined as

$$\boldsymbol{x} = \boldsymbol{\varphi}(\boldsymbol{X}) \quad \text{with} \quad \boldsymbol{F}(\boldsymbol{X}) := \nabla_{\boldsymbol{X}} \boldsymbol{\varphi}(\boldsymbol{X}) \tag{1}$$

being the macrodeformation gradient.[1] This second-order two-point tensor represents the gradient of the spatial-motion macrodeformation map $\boldsymbol{\varphi}$ with respect to material coordinates. The Jacobian determinant of the spatial-motion problem is denoted by $J := \det \boldsymbol{F} = \mathrm{d}v/\mathrm{d}V > 0$, with $\mathrm{d}V$ and $\mathrm{d}v$ being infinitesimal volume elements in the material and the spatial configuration, respectively. By introducing a second-order tensor $\bar{\boldsymbol{F}}$ which we refer to as the microdeformation map, we may express the affine deformation mapping from the material to the spatial configuration on the microscale as

$$\bar{\boldsymbol{x}} = \bar{\boldsymbol{F}}(\boldsymbol{X}) \cdot \bar{\boldsymbol{X}}, \quad \text{while } \bar{\boldsymbol{G}}(\boldsymbol{X}) := \nabla_{\boldsymbol{X}} \bar{\boldsymbol{F}}(\boldsymbol{X}) \tag{2}$$

defines the gradient of this microscale two-point tensor $\bar{\boldsymbol{F}}$ with respect to the material macroplacement and thus is a tensor of third order linking both scales.

2.1.2. Energy considerations and balance relations

For the prevailing quasi-static case, Dirichlet's principle is utilised, which requires the total potential energy to be stationary for the system to be in equilibrium. To achieve this, the variation of the total potential energy $\mathscr{E} = \int_{\mathscr{B}_0} U_0 \mathrm{d}V$ with respect to each of the kinematic quantities defined above at fixed material placement $\boldsymbol{X}$ is required to equal zero,[2]

$$\mathsf{D}_\delta \int_{\mathscr{B}_0} U_0(\boldsymbol{\varphi}, \boldsymbol{F}, \bar{\boldsymbol{F}}, \bar{\boldsymbol{G}}; \boldsymbol{X}) \mathrm{d}V = 0. \tag{3}$$

Herein U_0 denotes the total potential energy density per material unit volume $\mathrm{d}V$ in $\mathscr{B}_0$ and may be additively decomposed into its internal and external contributions, W_0 and V_0, respectively, as $U_0 = W_0 + V_0$. If we assume the material to behave hyperelastically, stresses can be defined as the derivatives of U_0 with respect to their particular energetically conjugate deformation variables at fixed material placement. Particularly, the spatial body force $\boldsymbol{b}_0$ acting on the material domain $\mathscr{B}_0$, as well the macrostress $\boldsymbol{P}$, microstress $\bar{\boldsymbol{P}}$ and the double-stress $\bar{\boldsymbol{Q}}$ of Piola type are obtained by the derivatives[3]:

$$\boldsymbol{b}_0 := -\partial_{\boldsymbol{\varphi}} U_0, \ \boldsymbol{P} := \mathsf{D}_{\boldsymbol{F}} U_0, \ \bar{\boldsymbol{P}} := \mathsf{D}_{\bar{\boldsymbol{F}}} U_0, \ \bar{\boldsymbol{Q}} := \mathsf{D}_{\bar{\boldsymbol{G}}} U_0. \tag{4}$$

The stresses $\boldsymbol{P}$ and $\bar{\boldsymbol{P}}$ are tensors of second order and $\bar{\boldsymbol{Q}}$ is of third order, respectively, and perform two-point description mappings as indicated in Fig. 2. With these in hand, (3) may be reformulated as the weak form of the balance of momentum:

$$\int_{\mathscr{B}_0} \left[\boldsymbol{P} : \delta \boldsymbol{F} + \bar{\boldsymbol{P}} : \delta \bar{\boldsymbol{F}} + \bar{\boldsymbol{Q}} \vdots \delta \bar{\boldsymbol{G}} - \boldsymbol{b}_0 \cdot \delta \boldsymbol{\varphi} \right] \mathrm{d}V = 0 \quad \forall \delta \boldsymbol{\varphi}, \delta \bar{\boldsymbol{F}}, \tag{5}$$

which must hold for arbitrary variations of $\delta\boldsymbol{\varphi}$ and $\delta\bar{\boldsymbol{F}}$. By application of divergence relations and the Gaussian theorem this equation is carried over to the local form of the balance of momentum[4]:

[1] The gradient of any quantity $\circ$ with respect to another quantity $\bullet$ is denoted by $\nabla_\bullet \circ = \frac{\partial \circ}{\partial \bullet}$.

[2] The variation of a quantity $\bullet$at fixed material placement $\boldsymbol{X}$ is represented by $\mathsf{D}_\delta \bullet$, while $\mathsf{d}_\delta \bullet$ denotes its variation at fixed spatial position $\boldsymbol{x}$.

[3] The derivatives of values with respect to tensors of any order are denoted by $\partial_\bullet \circ = \frac{\partial \circ}{\partial \bullet}$. Additionally for the sake of clarity, $\mathsf{D}_\bullet \circ = \frac{\partial \circ}{\partial \bullet}|_{\boldsymbol{X}}$ denotes the derivative with respect to a variable at fixed material placement $\boldsymbol{X}$ and $\mathsf{d}_\bullet \circ = \frac{\partial \circ}{\partial \bullet}|_{\boldsymbol{x}}$ the same at fixed spatial placement $\boldsymbol{x}$.

[4] The divergence operators identify as $\mathrm{Div} \bullet := \nabla_{\boldsymbol{X}}(\bullet) : \boldsymbol{I}$ and $\mathrm{div} \bullet := \nabla_{\boldsymbol{x}}(\bullet) : \boldsymbol{I}$, i.e., upper-case for the divergence with respect to material coordinates $\boldsymbol{X}$ and lower-case with respect to spatial coordinates $\boldsymbol{x}$.

$$\mathrm{Div}\ \boldsymbol{P} + \boldsymbol{b}_0 = \boldsymbol{0}, \quad \mathrm{Div}\ \bar{\boldsymbol{Q}} - \bar{\boldsymbol{P}} = \boldsymbol{0}, \tag{6}$$

which is constituted by one statement for the macro and another one for microscale and the corresponding homogeneous Neumann boundary conditions:

$$\boldsymbol{P} \cdot \boldsymbol{N} = \boldsymbol{0}, \quad \bar{\boldsymbol{Q}} \cdot \boldsymbol{N} = \boldsymbol{0}, \tag{7}$$

describing the macrotraction and the double-traction on the Neumann boundary $\partial\mathscr{B}_0^P$, $\partial\mathscr{B}_0^{\bar{Q}}$. Note that hereby without loss of generality any surface potential is omitted for the sake of simplicity, since otherwise the material-motion problem would become sophisticated. The local balances of momentum (6) may also be referred to as the Euler–Lagrange equations.

Remark 2.1. Upon setting $\bar{\boldsymbol{F}} \equiv \boldsymbol{F}$ and $\bar{\boldsymbol{G}} \equiv \boldsymbol{G} := \nabla_{\boldsymbol{X}}\boldsymbol{F}$ in Eq. (5), the weak form of the balance of momentum of a second-order gradient continuum is retrieved. The corresponding balance of momentum reads $\mathrm{Div}[\mathrm{D}_{\boldsymbol{F}}U_0 - \mathrm{Div}(\mathrm{D}_{\boldsymbol{G}}U_0)] - \boldsymbol{b}_0 = \boldsymbol{0}$.

2.1.3. Piola transform of the balance of momentum

As announced before, the present two-point formulation of the spatial-motion problem will be transferred to a purely spatial formulation as follows. A one-sided push forward – a Piola transformation – is applied to the balances of momentum (6) in order to rewrite them in terms of purely spatial stress tensors. These are of Cauchy type, namely the macrostress $\boldsymbol{\sigma}$, the microstress $\bar{\boldsymbol{\sigma}}$ and the double-stress $\bar{\boldsymbol{\tau}}$, which are illustrated in Fig. 3. For this purpose the Piola transformation formulae

$$\{\bullet\} \to j\{\bullet\} \cdot \boldsymbol{F}^{\mathrm{t}}, \quad \{\bullet\} \to j\{\bullet\} \cdot \bar{\boldsymbol{F}}^{\mathrm{t}}, \tag{8}$$

are employed for the macro and the microcontinuum, respectively. Using the inverse Jacobian determinant $j = 1/J = \mathrm{d}V/\mathrm{d}v$, (8) transforms the divergence operator $\mathrm{Div}(\bullet)$ with respect to material placement into the divergence operator with respect to spatial placement, $\mathrm{div}(\bullet)$. Finally, from $(8)_1$ we obtain the classical Piola identity $\boldsymbol{\sigma} = j\boldsymbol{P} \cdot \boldsymbol{F}^{\mathrm{t}}$. Moreover, the divergence relation $j\mathrm{Div}\,\bar{\boldsymbol{Q}} = \mathrm{div}\,(j\bar{\boldsymbol{Q}} \cdot \boldsymbol{F}^{\mathrm{t}})$ as well as the relation $j\boldsymbol{b}_0 = \boldsymbol{b}_t$ are exploited towards macro and the microbalance of momentum[5]:

$$\mathrm{div}\ \boldsymbol{\sigma} + \boldsymbol{b}_t = 0, \quad \mathrm{div}\ \bar{\boldsymbol{\tau}} - \bar{\boldsymbol{\sigma}} = 0. \tag{9}$$

in terms of the Cauchy-type stresses.

This evaluation renders the relations:[6,7]

$$\boldsymbol{\sigma} := j\boldsymbol{P} \cdot \boldsymbol{F}^{\mathrm{t}}, \quad \bar{\boldsymbol{\sigma}} := j\left[\bar{\boldsymbol{P}} \cdot \bar{\boldsymbol{F}}^{\mathrm{t}} + \bar{\boldsymbol{Q}} \overset{2;3}{\vdots} \bar{\boldsymbol{G}}\right], \quad \bar{\boldsymbol{\tau}} := j\bar{\boldsymbol{Q}} : \left[\bar{\boldsymbol{F}}^{\mathrm{t}} \overline{\otimes} \boldsymbol{F}^{\mathrm{t}}\right]. \tag{10}$$

between the Cauchy-type and the Piola-type stress measures of the spatial-motion problem. Furthermore $\boldsymbol{b}_t = -\partial_{\boldsymbol{\varphi}} U_t$ denotes the spatial body force per spatial unit volume $\mathrm{d}v$.

2.1.4. Spatial isotropy

In the case of spatial isotropy which coincides with the usual requirement of objectivity, the total energy density U_0 must be invariant under a rigid-body rotation by any proper orthogonal tensor $\boldsymbol{R}$ superposed onto the spatial configuration:

$$U_0 = U_0\left(\boldsymbol{F}, \bar{\boldsymbol{F}}, \bar{\boldsymbol{G}}, \bullet\right) \doteq U_0(\boldsymbol{R} \cdot \boldsymbol{F}, \boldsymbol{R} \cdot \bar{\boldsymbol{F}}, \boldsymbol{R} \cdot \bar{\boldsymbol{G}}, \bullet) \quad \forall \boldsymbol{R} \in \mathrm{SO}(3). \tag{11}$$

Upon a tedious analysis it follows that the sum $\boldsymbol{\sigma} + \bar{\boldsymbol{\sigma}}$ is symmetric. For a particular choice of constitutive equation, thus the relation

$$j\left[\boldsymbol{P} \cdot \boldsymbol{F}^{\mathrm{t}} + \bar{\boldsymbol{P}} \cdot \bar{\boldsymbol{F}}^{\mathrm{t}} + \bar{\boldsymbol{Q}} \overset{2;3}{\vdots} \bar{\boldsymbol{G}}\right] = j\left[\boldsymbol{F} \cdot \boldsymbol{P}^{\mathrm{t}} + \bar{\boldsymbol{F}} \cdot \bar{\boldsymbol{P}}^{\mathrm{t}} + \bar{\boldsymbol{G}} \overset{2;3}{\vdots} \bar{\boldsymbol{Q}}\right] \tag{12}$$

needs to be fulfilled in order to satisfy spatial isotropy. For further reference on this symmetry property, we suggest the contribution of Kirchner and Steinmann [12] and reference cited therein.

2.2. Material-motion problem – unde venis?

The same micromorphic continuum formulation is now discussed from the perspective of the material-motion problem.

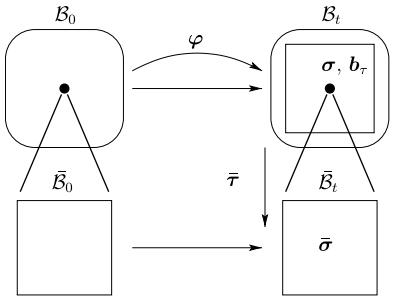

Fig. 3. Spatial-motion problem: Cauchy-type stress measures derived from Piola transform, $\tau = 0$, t.

[5] The Piola transformation formulas (8) applied to (6) yield (9) in the following manner:

$$j[\mathrm{Div}\ \boldsymbol{P} + \boldsymbol{b}_0] = j\ \mathrm{Div}(J\boldsymbol{\sigma} \cdot \boldsymbol{F}^{-\mathrm{t}}) + \boldsymbol{b}_t = \mathrm{div}\ \boldsymbol{\sigma} + \boldsymbol{b}_t,$$
$$j[\mathrm{Div}\ \bar{\boldsymbol{Q}} - \bar{\boldsymbol{P}}] \cdot \bar{\boldsymbol{F}}^{\mathrm{t}} = j\ \mathrm{Div}\left(J\bar{\boldsymbol{\tau}} : [\bar{\boldsymbol{F}}^{-\mathrm{t}} \overline{\otimes} \boldsymbol{F}^{-\mathrm{t}}]\right) \cdot \bar{\boldsymbol{F}}^{\mathrm{t}} - j\bar{\boldsymbol{P}} \cdot \bar{\boldsymbol{F}}^{\mathrm{t}} = \mathrm{div}\ \bar{\boldsymbol{\tau}} - \bar{\boldsymbol{\sigma}}.$$

[6] The regular and the modified dyadic products of two second-order tensors are defined through the relations

$$[\boldsymbol{A} \otimes \boldsymbol{B}] : \boldsymbol{C} = [\boldsymbol{B} : \boldsymbol{C}]\boldsymbol{A}, \quad \boldsymbol{A} : [\boldsymbol{B} \otimes \boldsymbol{C}] = [\boldsymbol{A} : \boldsymbol{B}]\boldsymbol{C},$$
$$[\boldsymbol{A} \overline{\otimes} \boldsymbol{B}] : \boldsymbol{C} = \boldsymbol{A} \cdot \boldsymbol{C} \cdot \boldsymbol{B}^{\mathrm{t}}, \quad \boldsymbol{A} : [\boldsymbol{B} \overline{\otimes} \boldsymbol{C}] = \boldsymbol{B}^{\mathrm{t}} \cdot \boldsymbol{A} \cdot \boldsymbol{C},$$
$$[\boldsymbol{A} \underline{\otimes} \boldsymbol{B}] : \boldsymbol{C} = \boldsymbol{A} \cdot \boldsymbol{C}^{\mathrm{t}} \cdot \boldsymbol{B}^{\mathrm{t}}, \quad \boldsymbol{A} : [\boldsymbol{B} \underline{\otimes} \boldsymbol{C}] = \boldsymbol{B}^{\mathrm{t}} \cdot \boldsymbol{A}^{\mathrm{t}} \cdot \boldsymbol{C}.$$

[7] Between two third-order tensors the product $\boldsymbol{A} \overset{i,j}{\vdots} \boldsymbol{B}$ symbolises the contraction over the ith and the jth index and thus yields a second-order tensor, while the product denoted by $\boldsymbol{A} \dot{:} \boldsymbol{B}$ means the contraction over all three indices and thus results in a scalar.

2.2.1. Kinematic relations

On the macroscale the material placement $\boldsymbol{X}$ of a physical point is treated as a function $\boldsymbol{\Phi}$ of its spatial placement $\boldsymbol{x}$. The deformation gradient of the macrocontinuum, $\boldsymbol{f}$, is defined as the gradient of the macrodeformation map $\boldsymbol{\Phi}$ with respect to the spatial placement $\boldsymbol{x}$,

$$\boldsymbol{X} = \boldsymbol{\Phi}(\boldsymbol{x}), \quad \boldsymbol{f}(\boldsymbol{x}) := \nabla_{\boldsymbol{x}} \boldsymbol{\Phi}(\boldsymbol{x}), \tag{13}$$

see Fig. 4. For the microcontinuum the deformation map $\bar{\boldsymbol{f}}$ and its gradient with respect to spatial coordinates $\boldsymbol{x}$, are introduced as

$$\bar{\boldsymbol{X}} = \bar{\boldsymbol{f}}(\boldsymbol{x}) \cdot \bar{\boldsymbol{x}}, \quad \bar{\boldsymbol{g}}(\boldsymbol{x}) := \nabla_{\boldsymbol{x}} \bar{\boldsymbol{f}}(\boldsymbol{x}). \tag{14}$$

The microdeformation map of the material-motion problem, $\bar{\boldsymbol{f}}$, is a two-point tensor of second order which performs a mapping from $\bar{\mathscr{B}}_t$ to $\bar{\mathscr{B}}_0$.

2.2.2. Energy considerations and balance relations

Within the material-motion problem, considerations along the lines of Dirichlet's principle must account for a *release of potential energy*, which must occur at any change in the material-motion problem kinematics, as implied by the second law of thermodynamics. Thus the variation of the total potential energy $\mathscr{E} = \int_{\mathscr{B}_t} U_t \mathrm{d}v$ with respect to the material-motion kinematic quantities at fixed spatial position $\boldsymbol{x}$ must be non-positive:

$$\mathrm{d}_{\delta}\mathscr{E} = \mathrm{d}_{\delta} \int_{\mathscr{B}_t} U_t(\boldsymbol{\Phi}, \boldsymbol{f}, \bar{\boldsymbol{f}}, \bar{\boldsymbol{g}}; \boldsymbol{x}) \mathrm{d}v \leqslant 0. \tag{15}$$

Herein U_t denotes the total potential-energy density with respect to the spatial unit volume $\mathrm{d}v$ in $\mathscr{B}_t$. Particularly, in case of configurational equilibrium, $\mathrm{d}_{\delta}\mathscr{E} = 0$, while in more general cases material traction quantities have to be considered:

$$\mathrm{d}_{\delta}\mathscr{E} =: \int_{\partial\mathscr{B}_t} \left[\mathrm{d}_{\delta}\boldsymbol{\Phi} \cdot \boldsymbol{T}_t^{p} + \mathrm{d}_{\delta}\bar{\boldsymbol{f}} : \boldsymbol{T}_t^{\bar{q}} \right] \mathrm{d}a. \tag{16}$$

Hereby a material macrotraction vector $\boldsymbol{T}_t^{p}$ and a material second-order double-traction tensor $\boldsymbol{T}_t^{\bar{q}}$ on the boundaries $\partial\mathscr{B}_t^{p}, \partial\mathscr{B}_t^{\bar{q}}$ enter as *definitions* and are energetically conjugate to both a variation of the macrodeformation map $\boldsymbol{\Phi}$ and the microdeformation map $\bar{\boldsymbol{f}}$, respectively.

In analogy to the spatial-motion problem, a material body force $\boldsymbol{B}_t$ acting on the spatial volume $\mathrm{d}v$ as well as a macrostress $\boldsymbol{p}$, a microstress $\bar{\boldsymbol{p}}$ and a double-stress $\bar{\boldsymbol{q}}$ of Piola

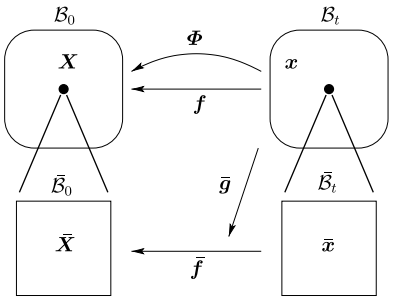

Fig. 4. Material-motion problem: micromorphic deformation maps.

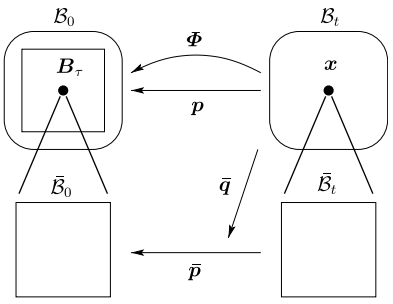

Fig. 5. Material-motion problem: Piola-type stress measures, $\tau = 0$, t.

type are introduced as the derivatives of U_t with respect to their energetically conjugate kinematic variables (compare Fig. 5):

$$\boldsymbol{B}_t := -\partial_{\boldsymbol{\Phi}} U_t, \quad \boldsymbol{p} := \mathrm{d}_{\boldsymbol{f}} U_t, \quad \bar{\boldsymbol{p}} := \mathrm{d}_{\bar{\boldsymbol{f}}} U_t, \quad \bar{\boldsymbol{q}} := \mathrm{d}_{\bar{\boldsymbol{g}}} U_t, \tag{17}$$

due to the underlying assumption of a hyperelastic material. The evaluation of the energy-release condition (16) directly results in the weak form of the material-motion balance of momentum:

$$\int_{\mathscr{B}_t} \left[\boldsymbol{p} : \delta\boldsymbol{f} + \bar{\boldsymbol{p}} : \delta\bar{\boldsymbol{f}} + \bar{\boldsymbol{q}} \vdots \delta\bar{\boldsymbol{g}} - \boldsymbol{B}_t \cdot \delta\boldsymbol{\Phi} \right] \mathrm{d}v =: \int_{\partial\mathscr{B}_t} \left[\boldsymbol{T}_t^{p} \cdot \delta\boldsymbol{\Phi} + \boldsymbol{T}_t^{\bar{q}} : \delta\bar{\boldsymbol{f}} \right] \mathrm{d}a. \tag{18}$$

This may again be locally expressed as the Euler–Lagrange equations

$$\mathrm{div}\, \boldsymbol{p} + \boldsymbol{B}_t = \boldsymbol{0}, \quad \mathrm{div}\, \bar{\boldsymbol{q}} - \bar{\boldsymbol{p}} = \boldsymbol{0}, \tag{19}$$

i.e., the balance of macro and micromomentum, which must be accompanied by the *non-homogeneous* Neumann boundary conditions

$$\boldsymbol{p} \cdot \boldsymbol{n} =: \boldsymbol{T}_t^{p}, \quad \bar{\boldsymbol{q}} \cdot \boldsymbol{n} =: \boldsymbol{T}_t^{\bar{q}}, \tag{20}$$

since any change in the material geometry at fixed spatial configuration directly yields non-zero material boundary tractions.

2.2.3. Piola transform of the balance of momentum

In an analogous manner to Section 2.1.3, for the material-motion problem the transition between the two-point description of the balance relations (19) and a purely material description can be achieved by applying the Piola transformation formulae

$$\{\bullet\} \to J\{\bullet\} \cdot \boldsymbol{f}^{\mathrm{t}}, \quad \{\bullet\} \to J\{\bullet\} \cdot \bar{\boldsymbol{f}}^{\mathrm{t}}, \tag{21}$$

which are here stated inversely to Eq. (8). With these at hand, we first obtain the divergence relations and the body force,

$$J\mathrm{div}\, \boldsymbol{p} = \mathrm{Div}(J\boldsymbol{p} \cdot \boldsymbol{f}^{\mathrm{t}}), \quad J\mathrm{div}\, \bar{\boldsymbol{q}} = \mathrm{Div}(J\bar{\boldsymbol{q}} \cdot \boldsymbol{f}^{\mathrm{t}}), \quad J\boldsymbol{B}_t = \boldsymbol{B}_0, \tag{22}$$

which finally yields the balance equations in the form:

$$\mathrm{Div}\, \boldsymbol{\Sigma} + \boldsymbol{B}_0 = \boldsymbol{0}, \quad \mathrm{Div}\, \bar{\boldsymbol{T}} - \bar{\boldsymbol{\Sigma}} = \boldsymbol{0} \tag{23}$$

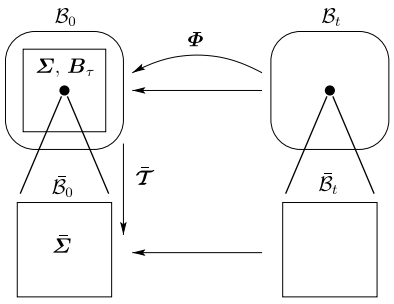

Fig. 6. Material-motion problem: Eshelby-type stress measures, $\tau = 0$, t.

in terms of the Eshelby-type – purely material – stress measures, i.e., the macrostress $\boldsymbol{\Sigma}$, the microstress $\bar{\boldsymbol{\Sigma}}$, and the double-stress $\bar{\boldsymbol{T}}$ as shown in Fig. 6. Along the derivation of Eq. (23), the relations:

$$\boldsymbol{\Sigma} := J\boldsymbol{p}\cdot\boldsymbol{f}^{\mathrm{t}}, \quad \bar{\boldsymbol{\Sigma}} := J\left[\bar{\boldsymbol{p}}\cdot\bar{\boldsymbol{f}}^{\mathrm{t}} + \bar{\boldsymbol{q}} \overset{2,3}{\vdots} \bar{\boldsymbol{g}}\right], \quad \bar{\boldsymbol{T}} := J\bar{\boldsymbol{q}} : \left[\bar{\boldsymbol{f}}^{\mathrm{t}}\overline{\otimes}\boldsymbol{f}^{\mathrm{t}}\right], \tag{24}$$

between the Eshelby-type material stress measures on the one hand and the two-point stress measures of Piola type on the other hand, become obvious.

2.2.4. Material isotropy

In the special case of material isotropy, i.e., the isotropy of the material response, the energy density U_t for the material-motion problem is invariant under a rigid-body rotation with any proper orthogonal tensor $\boldsymbol{r}$ superposed to the material configuration,

$$U_t = U_t(\boldsymbol{f},\bar{\boldsymbol{f}},\bar{\boldsymbol{g}},\bullet) \doteq U_t(\boldsymbol{r}\cdot\boldsymbol{f},\boldsymbol{r}\cdot\bar{\boldsymbol{f}},\boldsymbol{r}\cdot\bar{\boldsymbol{g}},\bullet) \quad \forall \boldsymbol{r} \in \mathrm{SO}(3). \tag{25}$$

Exploiting this condition, we conclude that the sum $\boldsymbol{\Sigma} + \bar{\boldsymbol{\Sigma}}$ is symmetric, i.e., $[\boldsymbol{\Sigma} + \bar{\boldsymbol{\Sigma}}] = [\boldsymbol{\Sigma} + \bar{\boldsymbol{\Sigma}}]^{\mathrm{t}}$.

2.3. Relations between spatial and material motion

In order to highlight the duality of the spatial- and the material-motion problem, conversions between the spatial- and the material-motion problem quantities are derived in the sequel.

2.3.1. Deformation maps and deformation gradients

The macrodeformation map of the spatial-motion problem, $\boldsymbol{\varphi}$ introduced in (1) and that of the material-motion problem, $\boldsymbol{\Phi}$, from Eq. (13) are inverse to each other, thus their compositions $\boldsymbol{\varphi}\circ\boldsymbol{\Phi} = \boldsymbol{i}\mathrm{d}$ and $\boldsymbol{\Phi}\circ\boldsymbol{\varphi} = \boldsymbol{i}\mathrm{d}$ yield the identity. Likewise, the macrodeformation gradient of the spatial- and that of the material-motion problem are related through $\boldsymbol{F}\cdot\boldsymbol{f} = \boldsymbol{I}_t$ and $\boldsymbol{f}\cdot\boldsymbol{F} = \boldsymbol{I}_0$ vice versa, while analogously the microdeformation maps compose as $\bar{\boldsymbol{F}}\cdot\bar{\boldsymbol{f}} = \bar{\boldsymbol{I}}_t$ and $\bar{\boldsymbol{f}}\cdot\bar{\boldsymbol{F}} = \bar{\boldsymbol{I}}_0$, respectively. Furthermore the Jacobians of the spatial- and the material-motion problem are related as $jJ = 1$. With these relations at hand the following expressions for the kinematic variables of the spatial-motion problem in terms of those from the material-motion problem are obtained for the macro and the microcontinuum quantities, respectively:

$$\boldsymbol{\varphi} = \boldsymbol{\Phi}^{-1}, \quad \boldsymbol{F} = \boldsymbol{f}^{-1}, \quad \bar{\boldsymbol{F}} = \bar{\boldsymbol{f}}^{-1}, \quad \bar{\boldsymbol{G}} = -\bar{\boldsymbol{F}}\cdot\bar{\boldsymbol{g}} : \left[\bar{\boldsymbol{F}}\overline{\otimes}\boldsymbol{F}\right]. \tag{26}$$

Vice versa the conversions from the spatial to the material-motion obey

$$\boldsymbol{\Phi} = \boldsymbol{\varphi}^{-1}, \quad \boldsymbol{f} = \boldsymbol{F}^{-1}, \quad \bar{\boldsymbol{f}} = \bar{\boldsymbol{F}}^{-1}, \quad \bar{\boldsymbol{g}} = -\bar{\boldsymbol{f}}\cdot\bar{\boldsymbol{G}} : \left[\bar{\boldsymbol{f}}\overline{\otimes}\boldsymbol{f}\right] \tag{27}$$

for the macro and the microcontinuum quantities, respectively.

2.3.2. Energy density

In the previous derivations, the stored energy densities U_0 and U_t were assigned to a particular perspective on the deformation. With the relations (26) and (27), we may however express these in terms of kinematic quantities either from the spatial- or from the material-motion problem. Particularly, for the stored energy density which is related to a material unit volume, the relation:

$$U_0(\boldsymbol{F},\bar{\boldsymbol{F}},\bar{\boldsymbol{G}}) = U_0\big(\boldsymbol{f},\bar{\boldsymbol{f}},\bar{\boldsymbol{g}}(\bar{\boldsymbol{G}},\bar{\boldsymbol{f}},\boldsymbol{f})\big) \tag{28}$$

holds. Analogously, we can transform the total stored energy density in the spatial configuration which is usually expressed in terms of material-motion quantities as follows:

$$U_t(\boldsymbol{f},\bar{\boldsymbol{f}},\bar{\boldsymbol{g}}) = U_t\big(\boldsymbol{F},\bar{\boldsymbol{F}},\bar{\boldsymbol{G}}(\bar{\boldsymbol{g}},\bar{\boldsymbol{F}},\boldsymbol{F})\big). \tag{29}$$

Furthermore the transformations between the stored energy density of the spatial and the material configuration, respectively, follow as

$$U_0 = JU_t \quad \text{and} \quad U_t = jU_0. \tag{30}$$

The relations of the partial derivative of the energy density with respect to a deformation measure at fixed material position to derivatives at fixed spatial position are computed as follows:

$$\begin{aligned}
\mathsf{D}_{\boldsymbol{f}}U_0 &= \mathsf{d}_{\boldsymbol{f}}U_0 : \partial_{\boldsymbol{f}}\boldsymbol{f} + \mathsf{d}_{\bar{\boldsymbol{f}}}U_0 : \partial_{\boldsymbol{f}}\bar{\boldsymbol{f}} + \mathsf{d}_{\bar{\boldsymbol{g}}}U_0 \vdots \partial_{\boldsymbol{f}}\bar{\boldsymbol{g}} \\
&= \mathsf{d}_{\boldsymbol{f}}U_0 + \mathsf{d}_{\bar{\boldsymbol{g}}}U_0 \vdots \partial_{\boldsymbol{f}}\bar{\boldsymbol{g}}, \\
\mathsf{D}_{\bar{\boldsymbol{f}}}U_0 &= \mathsf{d}_{\boldsymbol{f}}U_0 : \partial_{\bar{\boldsymbol{f}}}\boldsymbol{f} + \mathsf{d}_{\bar{\boldsymbol{f}}}U_0 : \partial_{\bar{\boldsymbol{f}}}\bar{\boldsymbol{f}} + \mathsf{d}_{\bar{\boldsymbol{g}}}U_0 \vdots \partial_{\bar{\boldsymbol{f}}}\bar{\boldsymbol{g}} \\
&= \mathsf{d}_{\bar{\boldsymbol{f}}}U_0 + \mathsf{d}_{\bar{\boldsymbol{g}}}U_0 \vdots \partial_{\bar{\boldsymbol{f}}}\bar{\boldsymbol{g}}, \\
\mathsf{D}_{\bar{\boldsymbol{g}}}U_0 &= \mathsf{d}_{\boldsymbol{f}}U_0 : \partial_{\bar{\boldsymbol{g}}}\boldsymbol{f} + \mathsf{d}_{\bar{\boldsymbol{f}}}U_0 : \partial_{\bar{\boldsymbol{g}}}\bar{\boldsymbol{f}} + \mathsf{d}_{\bar{\boldsymbol{g}}}U_0 \vdots \partial_{\bar{\boldsymbol{g}}}\bar{\boldsymbol{g}} \\
&= \mathsf{d}_{\bar{\boldsymbol{g}}}U_0,
\end{aligned} \tag{31}$$

while the reverse relations are obtained analogously as

$$\begin{aligned}
\mathsf{d}_{\boldsymbol{F}}U_t &= \mathsf{D}_{\boldsymbol{F}}U_t + \mathsf{D}_{\bar{\boldsymbol{G}}}U_t \vdots \partial_{\boldsymbol{F}}\bar{\boldsymbol{G}}, \\
\mathsf{d}_{\bar{\boldsymbol{F}}}U_t &= \mathsf{D}_{\bar{\boldsymbol{F}}}U_t + \mathsf{D}_{\bar{\boldsymbol{G}}}U_t \vdots \partial_{\bar{\boldsymbol{F}}}\bar{\boldsymbol{G}}, \\
\mathsf{d}_{\bar{\boldsymbol{G}}}U_t &= \mathsf{D}_{\bar{\boldsymbol{G}}}U_t.
\end{aligned} \tag{32}$$

These are in the following utilised to relate the spatial- and material-motion problem stresses to each other.

2.3.3. Push-forward of the stress measures from the spatial-motion problem

The Piola-type stresses $\boldsymbol{P} = \mathsf{D}_{\boldsymbol{F}} U_0$, $\bar{\boldsymbol{P}} = \mathsf{D}_{\bar{\boldsymbol{F}}} U_0$, and $\bar{\boldsymbol{Q}} = \mathsf{D}_{\bar{\boldsymbol{G}}} U_0$ in Eq. (4) of the spatial-motion problem enjoy the following relations:

$$\begin{aligned}
&\mathsf{D}_{\boldsymbol{F}} U_0 = \mathsf{D}_{\boldsymbol{f}} U_0 : \partial_{\boldsymbol{F}} \boldsymbol{f} = \mathsf{D}_{\boldsymbol{f}} U_0 : \left[-\boldsymbol{f} \overline{\otimes} \boldsymbol{f}^{\mathrm{t}}\right] = -\boldsymbol{f}^{\mathrm{t}} \cdot \mathsf{D}_{\boldsymbol{f}} U_0 \cdot \boldsymbol{f}^{\mathrm{t}},\\
&\mathsf{D}_{\bar{\boldsymbol{F}}} U_0 = \mathsf{D}_{\bar{\boldsymbol{f}}} U_0 : \partial_{\bar{\boldsymbol{F}}} \bar{\boldsymbol{f}} = \mathsf{D}_{\bar{\boldsymbol{f}}} U_0 : \left[-\bar{\boldsymbol{f}} \overline{\otimes} \bar{\boldsymbol{f}}^{\mathrm{t}}\right] = -\bar{\boldsymbol{f}}^{\mathrm{t}} \cdot \mathsf{D}_{\bar{\boldsymbol{f}}} U_0 \cdot \bar{\boldsymbol{f}}^{\mathrm{t}},\\
&\mathsf{D}_{\bar{\boldsymbol{G}}} U_0 = \mathsf{D}_{\bar{\boldsymbol{g}}} U_0 \vdots \partial_{\bar{\boldsymbol{G}}} \bar{\boldsymbol{g}} = \mathsf{D}_{\bar{\boldsymbol{g}}} U_0 \vdots \left[-\bar{\boldsymbol{f}} \underline{\otimes} \left[\bar{\boldsymbol{f}}^{\mathrm{t}} \overline{\otimes} \boldsymbol{f}^{\mathrm{t}}\right]\right]\\
&\qquad = -\bar{\boldsymbol{f}}^{\mathrm{t}} \cdot \mathsf{D}_{\bar{\boldsymbol{g}}} U_0 : \left[\bar{\boldsymbol{f}}^{\mathrm{t}} \overline{\otimes} \boldsymbol{f}^{\mathrm{t}}\right],
\end{aligned} \tag{33}$$

based on the relations (26). This fact may be exploited under consideration of the energy-density relations (28) and (31) as well as the Piola transform (8). Thus we obtain the relations:

$$\begin{aligned}
&j \mathsf{D}_{\boldsymbol{F}} U_0 \cdot \boldsymbol{F}^{\mathrm{t}} = -j \boldsymbol{f}^{\mathrm{t}} \cdot \mathsf{D}_{\boldsymbol{f}} U_0 = -j \boldsymbol{f}^{\mathrm{t}} \cdot \left[\mathsf{d}_{\boldsymbol{f}} U_0 + \mathsf{d}_{\bar{\boldsymbol{g}}} U_0 \vdots \partial_{\boldsymbol{f}} \bar{\boldsymbol{g}}\right],\\
&j \mathsf{D}_{\bar{\boldsymbol{F}}} U_0 \cdot \bar{\boldsymbol{F}}^{\mathrm{t}} = -j \bar{\boldsymbol{f}}^{\mathrm{t}} \cdot \mathsf{D}_{\bar{\boldsymbol{f}}} U_0 = -j \bar{\boldsymbol{f}}^{\mathrm{t}} \cdot \left[\mathsf{d}_{\bar{\boldsymbol{f}}} U_0 + \mathsf{d}_{\bar{\boldsymbol{g}}} U_0 \vdots \partial_{\bar{\boldsymbol{f}}} \bar{\boldsymbol{g}}\right],\\
&j \mathsf{D}_{\bar{\boldsymbol{G}}} U_0 : \left[\bar{\boldsymbol{F}}^{\mathrm{t}} \overline{\otimes} \boldsymbol{F}^{\mathrm{t}}\right] = -j \bar{\boldsymbol{f}}^{\mathrm{t}} \cdot \mathsf{D}_{\bar{\boldsymbol{g}}} U_0 = -\bar{\boldsymbol{f}}^{\mathrm{t}} \cdot \mathsf{d}_{\bar{\boldsymbol{g}}} U_t.
\end{aligned} \tag{34}$$

With these, the Cauchy-type spatial stress measures from the spatial-motion problem (10) expressed in terms of the Piola-type stress measures of the material-motion problem (17) read

$$\begin{aligned}
&\boldsymbol{\sigma} = U_t \boldsymbol{I} - \boldsymbol{f}^{\mathrm{t}} \cdot \boldsymbol{p} - \bar{\boldsymbol{g}} \overset{1,2}{\vdots} \bar{\boldsymbol{q}},\\
&\bar{\boldsymbol{\sigma}} = -\bar{\boldsymbol{f}}^{\mathrm{t}} \cdot \bar{\boldsymbol{p}} - \bar{\boldsymbol{g}} \overset{1,3}{\vdots} \bar{\boldsymbol{q}},\\
&\bar{\boldsymbol{\tau}} = -\bar{\boldsymbol{f}}^{\mathrm{t}} \cdot \bar{\boldsymbol{q}}.
\end{aligned} \tag{35}$$

2.3.4. Pull-back of the stress measures from the material-motion problem

In analogy to the previous subsection, a pull-back of the stress formats obtained in the material-motion problem can be executed. Using the relations (26) we may write:

$$\begin{aligned}
&\mathsf{d}_{\boldsymbol{f}} U_t = \mathsf{d}_{\boldsymbol{F}} U_t : \partial_{\boldsymbol{f}} \boldsymbol{F} = -\boldsymbol{F}^{\mathrm{t}} \cdot \mathsf{d}_{\boldsymbol{F}} U_t \cdot \boldsymbol{F}^{\mathrm{t}},\\
&\mathsf{d}_{\bar{\boldsymbol{f}}} U_t = \mathsf{d}_{\bar{\boldsymbol{F}}} U_t : \partial_{\bar{\boldsymbol{f}}} \bar{\boldsymbol{F}} = -\bar{\boldsymbol{F}}^{\mathrm{t}} \cdot \mathsf{d}_{\bar{\boldsymbol{F}}} U_t \cdot \bar{\boldsymbol{F}}^{\mathrm{t}},\\
&\mathsf{d}_{\bar{\boldsymbol{g}}} U_t = \mathsf{d}_{\bar{\boldsymbol{G}}} U_t \vdots \partial_{\bar{\boldsymbol{g}}} \bar{\boldsymbol{G}} = -\bar{\boldsymbol{F}}^{\mathrm{t}} \cdot \mathsf{d}_{\bar{\boldsymbol{G}}} U_t : \left[\bar{\boldsymbol{F}}^{\mathrm{t}} \overline{\otimes} \boldsymbol{F}^{\mathrm{t}}\right],
\end{aligned} \tag{36}$$

for the Piola-type stress quantities $\boldsymbol{p}$, $\bar{\boldsymbol{p}}$, and $\bar{\boldsymbol{q}}$ of (17). Furthermore we obtain the relations:

$$\begin{aligned}
&J \mathsf{d}_{\boldsymbol{f}} U_t \cdot \boldsymbol{f}^{\mathrm{t}} = -J \boldsymbol{F}^{\mathrm{t}} \cdot \mathsf{d}_{\boldsymbol{F}} U_t = -J \boldsymbol{F}^{\mathrm{t}} \cdot \left[\mathsf{D}_{\boldsymbol{F}} U_t + \mathsf{D}_{\bar{\boldsymbol{G}}} U_t \vdots \partial_{\boldsymbol{F}} \bar{\boldsymbol{G}}\right],\\
&J \mathsf{d}_{\bar{\boldsymbol{f}}} U_t \cdot \bar{\boldsymbol{f}}^{\mathrm{t}} = -J \bar{\boldsymbol{F}}^{\mathrm{t}} \cdot \mathsf{d}_{\bar{\boldsymbol{F}}} U_t = -J \bar{\boldsymbol{F}}^{\mathrm{t}} \cdot \left[\mathsf{D}_{\bar{\boldsymbol{F}}} U_t + \mathsf{D}_{\bar{\boldsymbol{G}}} U_t \vdots \partial_{\bar{\boldsymbol{F}}} \bar{\boldsymbol{G}}\right],\\
&J \mathsf{d}_{\bar{\boldsymbol{g}}} U_t : \left[\bar{\boldsymbol{f}}^{\mathrm{t}} \overline{\otimes} \boldsymbol{f}^{\mathrm{t}}\right] = -J \bar{\boldsymbol{F}}^{\mathrm{t}} \cdot \mathsf{D}_{\bar{\boldsymbol{G}}} U_t,
\end{aligned} \tag{37}$$

now departing from Eqs. (21), (30) and (32). Finally we end up with the material stress measures of Eshelby type from the material-motion problem, which particularly read

$$\begin{aligned}
&\boldsymbol{\Sigma} = U_0 \boldsymbol{I} - \boldsymbol{F}^{\mathrm{t}} \cdot \boldsymbol{P} - \bar{\boldsymbol{G}} \overset{1,2}{\vdots} \bar{\boldsymbol{Q}},\\
&\bar{\boldsymbol{\Sigma}} = -\bar{\boldsymbol{F}}^{\mathrm{t}} \cdot \bar{\boldsymbol{P}} - \bar{\boldsymbol{G}} \overset{1,3}{\vdots} \bar{\boldsymbol{Q}},\\
&\bar{\boldsymbol{T}} = -\bar{\boldsymbol{F}}^{\mathrm{t}} \cdot \bar{\boldsymbol{Q}}\cdot,
\end{aligned} \tag{38}$$

in terms of the Piola-type stress measures of the spatial-motion problem (4).

2.3.5. Push-forward and pull-back of the balance relations

The relations for the balance of momentum were originally derived in terms of stresses in two-point descriptions for both the spatial- and the material-motion problem, confer Sections 2.1 and 2.2. In both cases we applied Piola-transformation procedures in order obtain the respective purely spatial or purely material stress format and balance relations expressed in terms of these. Alternatively to this approach, one may also proceed directly from the two-point formulation of the spatial-motion problem, Section 2.1.2, to a fully material description in terms of Eshelby- type stresses by a pull-back operation, or analogously from the two-point formulation of the material-motion problem, Section 2.2.2, to a purely spatial description in terms of Cauchy-type stresses by a push-forward procedure.

Particularly, in order to move from the two-point description of the spatial-motion problem (6) to the purely material Eshelby-type description, the pull-back operations:

$$\begin{aligned}
&-\boldsymbol{F}^{\mathrm{t}} \cdot [\mathrm{Div}\ \boldsymbol{P} + \boldsymbol{b}_0] - \bar{\boldsymbol{G}} \overset{1,2}{\vdots} \left[\mathrm{Div}\ \bar{\boldsymbol{Q}} - \bar{\boldsymbol{P}}\right] = \mathrm{Div}\ \boldsymbol{\Sigma} + \boldsymbol{B}_0 = 0,\\
&-\bar{\boldsymbol{F}}^{\mathrm{t}} \cdot [\mathrm{Div}\ \bar{\boldsymbol{Q}} - \bar{\boldsymbol{P}}] = \mathrm{Div}\ \bar{\boldsymbol{T}} - \bar{\boldsymbol{\Sigma}} = 0,
\end{aligned} \tag{39}$$

are applied to the macro and the microterm of the balance relations and we directly obtain the expressions (23).

Analogously, the following push-forward operates on the material-motion problem balances (19) and yields the purely spatial description of the balance of momentum:

$$\begin{aligned}
&-\boldsymbol{f}^{\mathrm{t}} \cdot [\mathrm{div}\ \boldsymbol{p} + \boldsymbol{B}_t] - \bar{\boldsymbol{g}} \overset{1,2}{\vdots} [\mathrm{div}\ \bar{\boldsymbol{q}} - \bar{\boldsymbol{p}}] = \mathrm{div}\ \boldsymbol{\sigma} + \boldsymbol{b}_t = 0,\\
&-\bar{\boldsymbol{f}}^{\mathrm{t}} \cdot [\mathrm{div}\ \bar{\boldsymbol{q}} - \bar{\boldsymbol{p}}] = \mathrm{div}\ \bar{\boldsymbol{\tau}} - \bar{\boldsymbol{\sigma}} = 0,
\end{aligned} \tag{40}$$

in terms of stresses of Cauchy type as we also find it in Eq. (9).

2.3.6. Overall picture: balance-of-momentum tetragon

For the micromorphic continuum, the balance relations as derived for the spatial- and the material-motion problem in purely material respectively spatial quantities as well as in the respective two-point descriptions, may be summarised in a transformation scheme as shown in Fig. 7 where the elements of the balance relations are transformed either

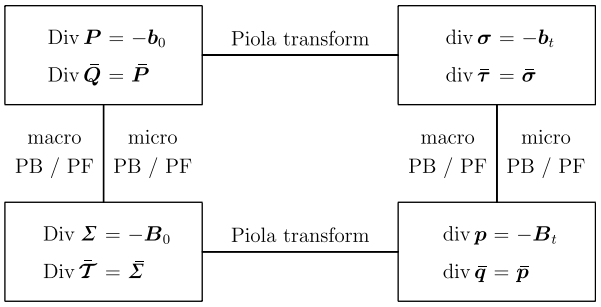

Fig. 7. Micromorphic balance-of-momentum tetragon.

with direct pull-back (PB) or push-forward (PF) operations or via Piola transformations.

3. Constitutive relations

In order to close the set of equations, a straightforward hyperelastic constitutive theory is chosen. Since the macro and the microcontinuum kinematically behave independently (compare Section 2), a constitutive formulation must be chosen to provide a relation between the scales. Thus in a straightforward manner, we have chosen to introduce a scale-transition term into the constitutive formulation. This formulation is first introduced for the spatial-motion problem and later transferred to the material-motion problem. The according stress measures are derived from this assumption for both perspectives and the symmetries imposed by spatial and material isotropy are shown.

3.1. Spatial-motion problem

3.1.1. Constitutive assumption for the stored-energy density

For the internally stored energy density W_0 we make the following hyperelastic constitutive ansatz

$$W_0 = \frac{1}{2}\lambda \ln^2 J + \frac{1}{2}\mu\big[\boldsymbol{F}:\boldsymbol{F} - n^{\dim} - 2\ln J\big] + \frac{1}{2}\mu l^2 \bar{\boldsymbol{G}} \vdots \bar{\boldsymbol{G}} + \frac{1}{2} p\big[\bar{\boldsymbol{F}} - \boldsymbol{F}\big] : \big[\bar{\boldsymbol{F}} - \boldsymbol{F}\big], \tag{41}$$

which consists of a Neo-Hooke-type term on the macroscale, a straightforward quadratic formulation on the microscale and an additional scale-transition term to couple both scales. Herein the material parameters λ and μ are the Lamé constants known from the classical or rather Boltzmann continuum. Additionally the so-called internal length l accounts for the scale dependence and may be interpreted as a characteristic size of the microcontinuum. The parameter p plays the part of a penalty which controls the interaction between the macro and the microdeformation. Furthermore $n^{\dim}$ denotes the number of dimensions in space. With the internal stored-energy density formulation, Eq. (41), the different stress fields may be evaluated, utilising the definitions (4) and the relations (10).

As shown in Kirchner and Steinmann [11] by constraining the micromorphic deformation such that the microdeformation map equals the macrodeformation gradient, the micromorphic continuum in its present formulation may be transferred to a second-order gradient continuum, since in the limit case of $p \to \infty$ we obtain $\bar{\boldsymbol{F}} \equiv \boldsymbol{F}$ and furthermore the gradient $\bar{\boldsymbol{G}} \equiv \nabla_{\boldsymbol{X}} \boldsymbol{F}$, see also Remark 2.1. Similar constitutive constraints on the kinematics as the one we have chosen have also been used by [25] as well as [14,16] for higher-order gradient theories and in their case have the major advantage of enabling C^0 approximation functions in the numerical implementation, since it reversely approaches a micromorphic continuum.

Remark 3.1. The scale transition in (41) can alternatively be obtained by a multiplicative formulation, i.e., $W_0^{\text{scale}} = p\big[\bar{\boldsymbol{f}} \cdot \boldsymbol{F} - \boldsymbol{I}\big] : \big[\bar{\boldsymbol{f}} \cdot \boldsymbol{F} - \boldsymbol{I}\big]$.

Note that the present choice is an assumption, and of course different formulations with a more complex relations could be used and can be considered as a challenge for future research.

3.1.2. Spatial-motion stresses

With the constitutive formulation (41) the Piola-type stresses (4) particularly result in

$$\begin{aligned} \boldsymbol{P} &= \mathsf{D}_{\boldsymbol{F}} W_0 = [\lambda \ln J - \mu]\boldsymbol{F}^{-\mathrm{t}} + \mu \boldsymbol{F} - p\big[\bar{\boldsymbol{F}} - \boldsymbol{F}\big], \\ \bar{\boldsymbol{P}} &= \mathsf{D}_{\bar{\boldsymbol{F}}} W_0 = p\big[\bar{\boldsymbol{F}} - \boldsymbol{F}\big], \\ \bar{\boldsymbol{Q}} &= \mathsf{D}_{\bar{\boldsymbol{G}}} W_0 = \mu l^2 \bar{\boldsymbol{G}}. \end{aligned} \tag{42}$$

Note that for a vanishing penalty parameter, i.e., $p \to 0$, the macrostress $\boldsymbol{P}$ and the double-stress $\bar{\boldsymbol{Q}}$ will be decoupled. Furthermore, we evaluate the Cauchy-type stresses as

$$\begin{aligned} \boldsymbol{\sigma} &= j\big[[\lambda \ln J - \mu]\boldsymbol{F}^{-\mathrm{t}} + \mu \boldsymbol{F} - p\big[\bar{\boldsymbol{F}} - \boldsymbol{F}\big]\big] \cdot \boldsymbol{F}^{\mathrm{t}}, \\ \bar{\boldsymbol{\sigma}} &= jp\big[\bar{\boldsymbol{F}} - \boldsymbol{F}\big] \cdot \bar{\boldsymbol{F}}^{\mathrm{t}} + j\mu l^2 \bar{\boldsymbol{G}} \overset{2,3}{\vdots} \bar{\boldsymbol{G}}, \\ \bar{\boldsymbol{\tau}} &= j\mu l^2 \bar{\boldsymbol{G}} : \big[\bar{\boldsymbol{F}}^{\mathrm{t}} \overline{\otimes} \boldsymbol{F}^{\mathrm{t}}\big], \end{aligned} \tag{43}$$

based on (10). Due to the scale-transition term, both the Cauchy-type macro and the microstress will generally be non-symmetric, with the degree of symmetry depending on the choice of the penalty parameter. As indicated before, in the case of spatial isotropy, however, the sum $\boldsymbol{\sigma} + \bar{\boldsymbol{\sigma}}$ is always symmetric.

3.2. Material-motion problem

3.2.1. Stored-energy density

Upon the assumption of zero external potential, i.e., $V_0 = 0$, which comes along with zero spatial body force, we may directly transfer the relation (30) of the total stored-energy density to the internal part, i.e., $W_t = jW_0$.

3.2.2. Material-motion stresses

For the application of the material force method, the stresses of the material-motion problem need to be evalu-

ated. From (17) with $U_t \equiv W_t$ and (41) we obtain the Piola-type stresses of the material-motion problem

$$\begin{aligned}\boldsymbol{p} &= j\Big[[W_0 - \lambda \ln J + \mu]\boldsymbol{I} - \mu \boldsymbol{F}^{\mathrm{t}} \cdot \boldsymbol{F} + p\boldsymbol{F}^{\mathrm{t}} \cdot \big[\bar{\boldsymbol{F}} - \boldsymbol{F}\big] \\ &\quad -\mu l^2 \bar{\boldsymbol{G}} \overset{1,2}{\vdots} \bar{\boldsymbol{G}}\Big] \cdot \boldsymbol{F}^{\mathrm{t}}, \\ \bar{\boldsymbol{p}} &= -jp\bar{\boldsymbol{F}}^{\mathrm{t}} \cdot \big[\bar{\boldsymbol{F}} - \boldsymbol{F}\big] \cdot \bar{\boldsymbol{F}}^{\mathrm{t}}, \\ \bar{\boldsymbol{q}} &= -j\mu l^2 \bar{\boldsymbol{F}}^{\mathrm{t}} \cdot \bar{\boldsymbol{G}} : \bar{\boldsymbol{F}}^{\mathrm{t}} \overline{\otimes} \boldsymbol{F}^{\mathrm{t}},\end{aligned} \tag{44}$$

from which the Eshelby-type stresses are evaluated as

$$\begin{aligned}\boldsymbol{\Sigma} &= [W_0 - \lambda \ln J + \mu]\boldsymbol{I} - \mu \boldsymbol{F}^{\mathrm{t}} \cdot \boldsymbol{F} + p\boldsymbol{F}^{\mathrm{t}} \cdot \big[\bar{\boldsymbol{F}} - \boldsymbol{F}\big] \\ &\quad - \mu l^2 \bar{\boldsymbol{G}} \overset{1,2}{\vdots} \bar{\boldsymbol{G}}, \\ \bar{\boldsymbol{\Sigma}} &= -p\bar{\boldsymbol{F}}^{\mathrm{t}} \cdot \big[\bar{\boldsymbol{F}} - \boldsymbol{F}\big] - \mu l^2 \bar{\boldsymbol{G}} \overset{1,3}{\vdots} \bar{\boldsymbol{G}}, \\ \bar{\boldsymbol{T}} &= -\mu l^2 \bar{\boldsymbol{F}}^{\mathrm{t}} \cdot \bar{\boldsymbol{G}},\end{aligned} \tag{45}$$

utilising (24).

For this particular choice of stresses, the symmetry of the sum of the Eshelby-type macro and the microstress, $\boldsymbol{\Sigma} + \bar{\boldsymbol{\Sigma}}$, resulting from material isotropy as stated in Eq. (25) can be shown. Observing

$$\begin{aligned}\boldsymbol{\Sigma} + \bar{\boldsymbol{\Sigma}} &= [W_0 - \lambda \ln J + \mu]\boldsymbol{I} - \mu \boldsymbol{F}^{\mathrm{t}} \cdot \boldsymbol{F} + p\boldsymbol{F}^{\mathrm{t}} \cdot \bar{\boldsymbol{F}} - p\boldsymbol{F}^{\mathrm{t}} \cdot \boldsymbol{F} \\ &\quad - p\bar{\boldsymbol{F}}^{\mathrm{t}} \cdot \bar{\boldsymbol{F}} + p\bar{\boldsymbol{F}}^{\mathrm{t}} \cdot \boldsymbol{F} - \mu l^2 \Big[\bar{\boldsymbol{G}} \overset{1,2}{\vdots} \bar{\boldsymbol{G}}\Big] - \mu l^2 \Big[\bar{\boldsymbol{G}} \overset{1,3}{\vdots} \bar{\boldsymbol{G}}\Big],\end{aligned} \tag{46}$$

we notice that $\boldsymbol{\Sigma} + \bar{\boldsymbol{\Sigma}} = [\boldsymbol{\Sigma} + \bar{\boldsymbol{\Sigma}}]^{\mathrm{t}}$ and thus the symmetry is fulfilled.

4. Finite-element approximation

For the continuum theory presented in Section 2 a finite-element approximation scheme is derived in a general format for which then the constitutive formulation of Section 3 is incorporated. For the finite-element approximation we chose the macro and the microdeformation map as the unknown quantities to be solved for.

4.1. Spatial-motion problem

The unknown fields of the deformation quantities are approximated using a standard Bubnov–Galerkin approach which allows to use the same interpolation functions for the unknowns as well as for the test functions. Particularly, a finite-element mesh consists of n_φ nodes at which the macrodeformation map $\boldsymbol{\varphi}$ is evaluated and $n_{\bar{F}}$ nodes for the unknown microdeformation map $\bar{\boldsymbol{F}}$. Globally their approximations are formulated with shape functions N_L^φ for the deformation and $N_M^{\bar{F}}$ for the microdeformation map, respectively as

$$\begin{aligned}\boldsymbol{\varphi}^h &= \sum_{L=1}^{n_\varphi} N_L^\varphi \boldsymbol{\varphi}_L, \quad \delta\boldsymbol{\varphi}^h = \sum_{I=1}^{n_\varphi} N_I^\varphi \delta\boldsymbol{\varphi}_I, \\ \bar{\boldsymbol{F}}^h &= \sum_{M=1}^{n_{\bar{F}}} N_M^{\bar{F}} \bar{\boldsymbol{F}}_M, \quad \delta\bar{\boldsymbol{F}}^h = \sum_{J=1}^{n_{\bar{F}}} N_J^{\bar{F}} \delta\bar{\boldsymbol{F}}_J.\end{aligned} \tag{47}$$

Herein the nodal indices I and L account for the discrete values of the unknown $\boldsymbol{\varphi}$ and its variation, while J and M number the nodes for unknown $\bar{\boldsymbol{F}}$ and their variation, respectively. Accordingly, the discrete approximations for the gradient variables $\boldsymbol{F} = \nabla_{\boldsymbol{X}}\boldsymbol{\varphi}$ and $\bar{\boldsymbol{G}} = \nabla_{\boldsymbol{X}}\bar{\boldsymbol{F}}$ and their respective variations $\delta\boldsymbol{F} = \nabla_{\boldsymbol{X}}\delta\boldsymbol{\varphi}$ and $\delta\bar{\boldsymbol{G}} = \nabla_{\boldsymbol{X}}\delta\bar{\boldsymbol{F}}$ read

$$\begin{aligned}\boldsymbol{F}^h &= \sum_{L=1}^{n_\varphi} \boldsymbol{\varphi}_L \otimes \nabla_{\boldsymbol{X}} N_L^\varphi, \quad \delta\boldsymbol{F}^h = \sum_{I=1}^{n_\varphi} \delta\boldsymbol{\varphi}_I \otimes \nabla_{\boldsymbol{X}} N_I^\varphi, \\ \bar{\boldsymbol{G}}^h &= \sum_{M=1}^{n_{\bar{F}}} \bar{\boldsymbol{F}}_M \otimes \nabla_{\boldsymbol{X}} N_M^{\bar{F}}, \quad \delta\bar{\boldsymbol{G}}^h = \sum_{J=1}^{n_{\bar{F}}} \delta\bar{\boldsymbol{F}}_J \otimes \nabla_{\boldsymbol{X}} N_J^{\bar{F}}.\end{aligned} \tag{48}$$

Maintaining the assumption of zero body forces, the discrete residuals of the spatial-motion problem read

$$\begin{aligned}\mathbf{R}_I^\varphi &= \int_{\mathscr{B}_0} \boldsymbol{P} \cdot \nabla_{\boldsymbol{X}} N_I^\varphi \mathrm{d}V \quad - \mathbf{F}_I^{\varphi\mathrm{ext}} \overset{!}{=} 0, \\ \mathbf{R}_J^{\bar{F}} &= \int_{\mathscr{B}_0} \bar{\boldsymbol{Q}} \cdot \nabla_{\boldsymbol{X}} N_J^{\bar{F}} \mathrm{d}V + \int_{\mathscr{B}_0} \bar{\boldsymbol{P}} N_J^{\bar{F}} \mathrm{d}V - \mathbf{F}_J^{\bar{F}\mathrm{ext}} \overset{!}{=} 0,\end{aligned} \tag{49}$$

wherein the Piola-type stresses $\boldsymbol{P}$, $\bar{\boldsymbol{P}}$, and $\bar{\boldsymbol{Q}}$ are determined by (42). Consequently the linearised coupled problem

$$\begin{bmatrix} \mathbf{K}_{IL}^{\varphi\varphi} & \mathbf{K}_{IM}^{\varphi\bar{F}} \\ \mathbf{K}_{JL}^{\bar{F}\varphi} & \mathbf{K}_{JM}^{\bar{F}\bar{F}} \end{bmatrix} \begin{bmatrix} \Delta\boldsymbol{\varphi}_L^h \\ \Delta\bar{\boldsymbol{F}}_M^h \end{bmatrix} = \begin{bmatrix} \mathbf{F}_I^{\varphi\mathrm{ext}} - \mathbf{F}_I^{\varphi\mathrm{int}} \\ \mathbf{F}_J^{\bar{F}\mathrm{ext}} - \mathbf{F}_J^{\bar{F}\mathrm{int}} \end{bmatrix},$$

is to be solved for increments of $\boldsymbol{\varphi}_L^h$ and $\bar{\boldsymbol{F}}_M^h$. The component matrices of the global tangent stiffness matrix are given by

$$\begin{aligned}\mathbf{K}_{IL}^{\varphi\varphi} &= \frac{\partial \mathbf{R}_I^\varphi}{\partial \boldsymbol{\varphi}_L} = \int_{\mathscr{B}_0} \mathsf{D}_{\boldsymbol{F}}(\boldsymbol{P} \cdot \nabla_{\boldsymbol{X}} N_I^\varphi) \cdot \nabla_{\boldsymbol{X}} N_L^\varphi \mathrm{d}V, \\ \mathbf{K}_{IM}^{\varphi\bar{F}} &= \frac{\partial \mathbf{R}_I^\varphi}{\partial \bar{\boldsymbol{F}}_M} = \int_{\mathscr{B}_0} \mathsf{D}_{\bar{\boldsymbol{F}}}(\boldsymbol{P} \cdot \nabla_{\boldsymbol{X}} N_I^\varphi) N_M^{\bar{F}} \mathrm{d}V, \\ \mathbf{K}_{JL}^{\bar{F}\varphi} &= \frac{\partial \mathbf{R}_J^{\bar{F}}}{\partial \boldsymbol{\varphi}_L} = \int_{\mathscr{B}_0} \mathsf{D}_{\boldsymbol{F}}(\bar{\boldsymbol{Q}} \cdot \nabla_{\boldsymbol{X}} N_J^{\bar{F}}) \cdot \nabla_{\boldsymbol{X}} N_L^\varphi \mathrm{d}V \\ &\quad + \int_{\mathscr{B}_0} \mathsf{D}_{\boldsymbol{F}}(\bar{\boldsymbol{P}} N_J^{\bar{F}}) \cdot \nabla_{\boldsymbol{X}} N_L^\varphi \mathrm{d}V, \\ \mathbf{K}_{JM}^{\bar{F}\bar{F}} &= \frac{\partial \mathbf{R}_J^{\bar{F}}}{\partial \bar{\boldsymbol{F}}_M} = \int_{\mathscr{B}_0} \mathsf{D}_{\bar{\boldsymbol{G}}}(\bar{\boldsymbol{Q}} \cdot \nabla_{\boldsymbol{X}} N_J^{\bar{F}}) \cdot \nabla_{\boldsymbol{X}} N_M^{\bar{F}} \mathrm{d}V \\ &\quad + \int_{\mathscr{B}_0} \mathsf{D}_{\bar{\boldsymbol{F}}}(\bar{\boldsymbol{P}} N_J^{\bar{F}}) N_M^{\bar{F}} \mathrm{d}V.\end{aligned} \tag{50}$$

Herein the specific tangent operators for the constitutive law of Section 3 read

$$\begin{aligned}&\mathsf{D}_{\boldsymbol{F}}\boldsymbol{P} = \lambda \boldsymbol{F}^{-\mathrm{t}} \otimes \boldsymbol{F}^{-\mathrm{t}} - [\lambda \ln J - \mu]\boldsymbol{F}^{-\mathrm{t}} \underline{\otimes} \boldsymbol{F}^{-1} + [\mu + p]\boldsymbol{I} \overline{\otimes} \boldsymbol{I}, \\ &\mathsf{D}_{\bar{\boldsymbol{F}}}\boldsymbol{P} = \mathsf{D}_{\boldsymbol{F}}\bar{\boldsymbol{P}} = -p\boldsymbol{I} \overline{\otimes} \boldsymbol{I}, \quad \mathsf{D}_{\bar{\boldsymbol{F}}}\bar{\boldsymbol{P}} = +p\boldsymbol{I} \overline{\otimes} \boldsymbol{I}, \\ &\mathsf{D}_{\bar{\boldsymbol{G}}}\bar{\boldsymbol{Q}} = +\mu l^2 \boldsymbol{I} \underline{\otimes} [\boldsymbol{I} \overline{\otimes} \boldsymbol{I}], \quad \mathsf{D}_{\boldsymbol{F}}\bar{\boldsymbol{Q}} = 0.\end{aligned} \tag{51}$$

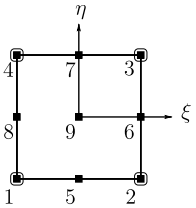

Fig. 8. Isoparametric quadrilateral master element with 9 nodes for the macrodeformation map and 4 nodes for the microdeformation map.

Particularly, $\mathsf{D}_{\boldsymbol{F}}\boldsymbol{P}$, $\mathsf{D}_{\bar{\boldsymbol{F}}}\boldsymbol{P}$, $\mathsf{D}_{\boldsymbol{F}}\bar{\boldsymbol{P}}$, and $\mathsf{D}_{\bar{\boldsymbol{F}}}\bar{\boldsymbol{P}}$ are fourth-order tensors; $\mathsf{D}_{\boldsymbol{G}}\bar{\boldsymbol{Q}}$ represents a tensor of sixth order, while the fifth-order tensor $\mathsf{D}_{\boldsymbol{F}}\bar{\boldsymbol{Q}}$ vanishes for the present formulation.

The actual implementation is done element-wise with assembly to a global system of equations as in standard finite-element procedures. Also the standard procedure of Gauss quadrature is used for the numerical evaluation of the integrals above.

The constitutive law of Section 3, which incorporates the difference between the microdeformation map $\bar{\boldsymbol{F}}$ and the macrotangent map $\boldsymbol{F}$, necessitates the use of shape functions of different order in the finite-element approximation. A detailed reference for the suitability of different kinds of elements for such formulations can be found in Refs. [14,16], see also [25,1]. Particularly, we have chosen quadrilateral plane elements with a bi-quadratic approximation for the macrodeformation map $\boldsymbol{\varphi}$ and a bi-linear approximation for the microdeformation map $\bar{\boldsymbol{F}}$ as shown in Fig. 8.

4.2. Material-motion problem

Accordingly, the approximations of the unknown quantities of the material-motion problem, the macrodeformation map $\boldsymbol{\Phi}$ and the microdeformation map $\bar{\boldsymbol{f}}$, are formulated in terms of the material-motion shape functions N^{Φ}_{L} and $N^{\bar{f}}_{M}$, respectively, as

$$\begin{aligned}\boldsymbol{\Phi}^h &= \sum_{L=1}^{n_\Phi} N^{\Phi}_{L}\boldsymbol{\Phi}_L, \quad \delta\boldsymbol{\Phi}^h = \sum_{I=1}^{n_\Phi} N^{\Phi}_{I}\delta\boldsymbol{\Phi}_I,\\ \bar{\boldsymbol{f}}^h &= \sum_{M=1}^{n_{\bar{f}}} N^{\bar{f}}_{M}\bar{\boldsymbol{f}}_M, \quad \delta\bar{\boldsymbol{f}}^h = \sum_{J=1}^{n_{\bar{f}}} N^{\bar{f}}_{J}\delta\bar{\boldsymbol{f}}_J.\end{aligned} \tag{52}$$

Herein, $N^{\Phi}_{L} \equiv N^{\varphi}_{L}$ and $N^{\bar{f}}_{M} \equiv N^{\bar{F}}_{M}$, but here the gradients are derived with respect to the spatial coordinates. Particularly, $\boldsymbol{f} = \nabla_{\boldsymbol{x}}\boldsymbol{\Phi}$ and $\bar{\boldsymbol{g}} = \nabla_{\boldsymbol{x}}\bar{\boldsymbol{f}}$ and their respective variations read

$$\begin{aligned}\boldsymbol{f}^h &= \sum_{L=1}^{n_\Phi} \boldsymbol{\Phi}_L \otimes \nabla_{\boldsymbol{x}} N^{\Phi}_{L}, \quad \delta\boldsymbol{f}^h = \sum_{I=1}^{n_\Phi} \delta\boldsymbol{\Phi}_I \otimes \nabla_{\boldsymbol{x}} N^{\Phi}_{I},\\ \bar{\boldsymbol{g}}^h &= \sum_{M=1}^{n_{\bar{f}}} \bar{\boldsymbol{f}}_M \otimes \nabla_{\boldsymbol{x}} N^{\bar{f}}_{M}, \quad \delta\bar{\boldsymbol{g}}^h = \sum_{J=1}^{n_{\bar{f}}} \delta\bar{\boldsymbol{f}}_J \otimes \nabla_{\boldsymbol{x}} N^{\bar{f}}_{J}.\end{aligned} \tag{53}$$

With these test and trial functions in hand, we may now apply the material force method to our micromorphic continuum in the spirit of, for instance [30,18].

4.2.1. Material force method for the material balance of macromomentum

From the integral version of the balance of momentum for the macrocontinuum we obtain $(19)_1$,

$$\int_{\mathscr{B}_t} \delta\boldsymbol{\Phi}\cdot[\operatorname{div}\boldsymbol{p} + \boldsymbol{B}_t]\mathrm{d}v = 0 \quad \forall\ \delta\boldsymbol{\Phi} \tag{54}$$

wherein the body force is kept here for the sake of completeness. For arbitrary variations $\delta\boldsymbol{\Phi}$ and with the finite-element approximations $(52)_1$ and $(53)_1$ we obtain a quantity that we define as the *nodal material force* of the macroscale:

$$\mathfrak{F}_L := \int_{\mathscr{B}_t} [\boldsymbol{p}\cdot\nabla_{\boldsymbol{x}} N^{\Phi}_{L} - \boldsymbol{B}_t N^{\Phi}_{L}]\mathrm{d}v. \tag{55}$$

This force vector acts on the material manifold and is energetically conjugate to the material virtual node-point displacements at node L, $\delta\boldsymbol{\Phi}_L$. The material force $\mathfrak{F}_L$ exclusively concerns the macromomentum and thus appears in the same format as for a classical or rather Boltzmann continuum.

Remark 4.1. The material force may be equally derived in terms of the purely material stresses of Eshelby type

$$\int_{\mathscr{B}_0} \delta\boldsymbol{\Phi}\cdot J[\operatorname{div}\boldsymbol{p} + \boldsymbol{B}_t]\mathrm{d}V = \int_{\mathscr{B}_0} \delta\boldsymbol{\Phi}\cdot[\operatorname{Div}\boldsymbol{\Sigma} + \boldsymbol{B}_0]\mathrm{d}V = 0,$$

from the pull back and by execution of the Piola transformation (21).

4.2.2. Material force method for the material balance of micromomentum

For the sake of completeness, we attempt to obtain a comparable nodal configurational double-traction based on the material balance of the micromomentum. Thus the material-motion balance of $(19)_2$ is brought into a weak form,

$$\int_{\mathscr{B}_t} \delta\bar{\boldsymbol{f}} : [\operatorname{div}\bar{\boldsymbol{q}} - \bar{\boldsymbol{p}}]\mathrm{d}v = 0, \tag{56}$$

by multiplication with the virtual microdeformation map $\delta\bar{\boldsymbol{f}}$ of the material-motion problem. From this we obtain what we call a *nodal configurational double-force* which in the discretised version with the approximations $(52)_2$ and $(53)_2$ reads

$$\bar{\mathfrak{m}}_J := \int_{\mathscr{B}_t} \left[\bar{\boldsymbol{q}}\cdot\nabla_{\boldsymbol{x}} N^{\bar{f}}_{J} + \bar{\boldsymbol{p}} N^{\bar{f}}_{J}\right]\mathrm{d}v. \tag{57}$$

This discrete configurational micro double-force is energetically conjugate to the microdeformation map $\bar{\boldsymbol{f}}$ of the material-motion problem and discretely evaluated at the nodes of the finite-element mesh. Contrary to the material force $\mathfrak{F}_L$ the configurational micro double-force $\bar{\mathfrak{m}}_J$ is a non-symmetric two-point tensor.

Remark 4.2. Alternatively the configurational micro double-force can be expressed in terms of Eshelby-type stresses

by executing a pull-back and a Piola-transformation on the microbalance of momentum (56):

$$\int_{\mathscr{B}_0} \left[J[\operatorname{div} \bar{\boldsymbol{q}} - \bar{\boldsymbol{p}}] \cdot \bar{\boldsymbol{f}}^{\mathrm{t}}\right] : \left[\delta\bar{\boldsymbol{f}} \cdot \bar{\boldsymbol{F}}\right] \mathrm{d}V = \int_{\mathscr{B}_0} \left[\operatorname{Div} \bar{\boldsymbol{T}} - \bar{\boldsymbol{\Sigma}}\right] : \left[\delta\bar{\boldsymbol{f}} \cdot \bar{\boldsymbol{F}}\right] \mathrm{d}V = 0.$$

5. Numerical examples

The above proposed algorithm for the micromorphic continuum is now applied to two selected numerical examples. First, a finite-element solution for the spatial-motion problem is obtained according to Section 4.1 in a two-point formulation. From the directly obtained nodal values for $\boldsymbol{\varphi}$ and $\bar{\boldsymbol{F}}$, all other kinematic quantities can be derived (compare Section 2.3). With these at hand, for instance all presented stress fields can be evaluated using the relations of Sections 3.1.2 and 3.2.2. The material force method, which was presented in Section 4.2 for the micromorphic continuum, is employed to obtain the material forces and configurational double-forces of the micromorphic continuum.

The response is studied at two different boundary value problems: The first geometry under consideration is a specimen with a circular hole under uniaxial loading, while the second one is a rectangularly shaped specimen with a static crack under mode-I loading. Both geometries are discretised with the finite elements of Section 4.1 and Fig. 8. The boundary conditions applied consist of non-homogeneous Dirichlet and homogeneous Neumann boundary conditions for the macrodeformation map as well as homogeneous Neumann boundary conditions for the microdeformation map.

5.1. Uniaxial loading of specimen with hole

Into the rectangular specimen of length L_0 and width $L_0/3$, an inhomogeneity is introduced by means of a centred circular hole of radius $r = L_0/12$, as shown in Fig. 9.

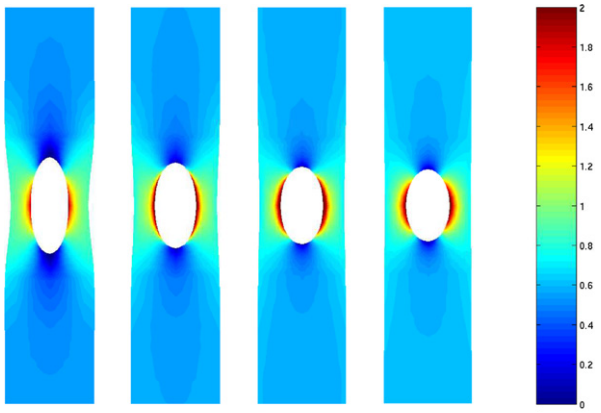

Fig. 9. Cauchy-type macrostress σ_{22} at variation of the internal length at $p = 20\,E$.

While the nodes at the bottom edge of the discretised geometry are fixed in longitudinal direction, a constant displacement boundary condition in the same direction is applied on the top nodes step-wise until the final length of $1.5\,L_0$ is reached.

5.1.1. Results from the spatial-motion problem

The internal length l is varied for fixed scale-transition parameter $p = 20\,E$ in order to firstly investigate the resulting field of the normal Cauchy-type macrostress σ_{22} in loading direction, and secondly the scale-transition term $\|\bar{\boldsymbol{F}} - \boldsymbol{F}\|^2$ of the internal stored energy density (41).

Fig. 9 shows the distribution of the Cauchy-type macrostress component σ_{22} for different internal length ratios and a fixed scale-transition parameter $p = 20\,E$ plotted in the spatial mesh. The first aspect to observe is that the overall behaviour of the specimen becomes stiffer with increasing internal length, i.e. the deformation of the hole is less distinct compared to the overall deformation. Moreover, the stress field is influenced more distinctively in a wider region by the inhomogeneity represented by the hole. Especially the first effect can be attributed to an increased stiffness in the microterm of Eq. (41) at increasing the internal-length parameter l.

In Fig. 10 we compare the stress components of the Cauchy-type macrostress for two different internal lengths. For zero internal length, the fields appear symmetric while for the larger internal length of $l = L_0/6$ the non-symmetry of the tensor $\boldsymbol{\sigma}$ is revealed. This coincides with a non-symmetric macrostress tensor generally predicted by the literature for non-local formulations.

Now the influence of the internal length on the scale-transition term is investigated. Its contour is displayed in Fig. 11 for varied internal length l at fixed scale-transition parameter $p = 20\,E$. Herein mainly the shape of the region with a significantly large term $\|\bar{\boldsymbol{F}} - \boldsymbol{F}\|^2$ differs with

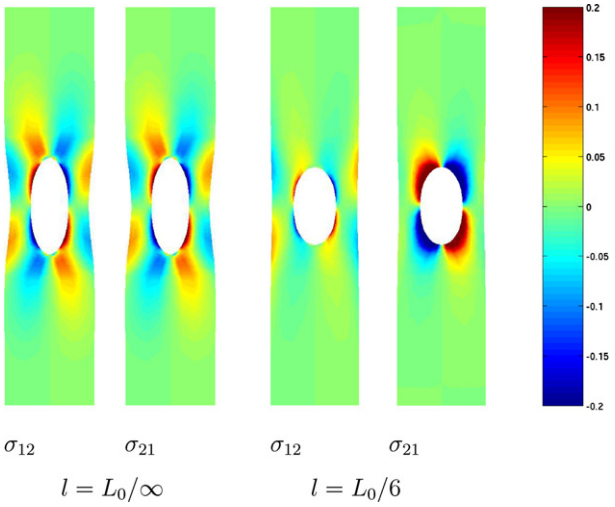

Fig. 10. Shear components of the Cauchy-type macrostress, σ_{12} and σ_{21}, in comparison for two different internal lengths $l = L_0/\infty$ and $l_0 = L_0/6$ at $p = 20\,E$.

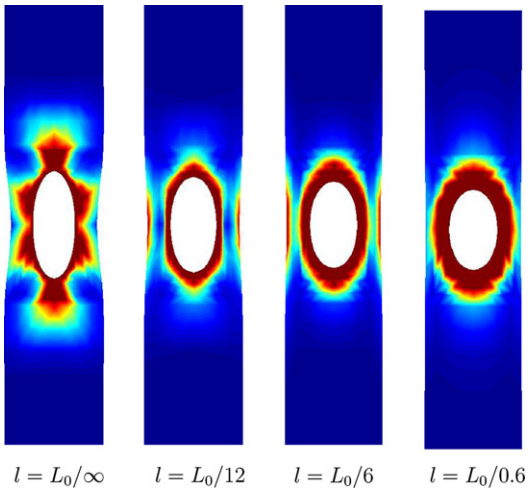

Fig. 11. Scale-transition measure $\|\bar{\boldsymbol{F}} - \boldsymbol{F}\|^2$ at variation of the internal length at $p = 20\,E$.

increasing internal length: For larger l, the term appears more restricted to the direct circumference of the hole but less effectively controlled by the parameter p. For explanation of these effects, one may point to the fact that for zero internal length, no microstructural effects are incorporated. As the microdeformation map $\bar{\boldsymbol{F}}$ vanishes, the scale-transition term is of the order of the macrodeformation gradient $\boldsymbol{F}$ and therefore has no decisive significance. Otherwise, if $l > 0$, the influence of the scale-transition term becomes larger and also more closely aligned along the edge of the hole due to stronger microdeformation.

5.1.2. Results from the material-motion problem

In the sequel, the material force method is applied to the current boundary- value problem. In particular, the nodal material forces at the finite-element nodes as well as the nodal configurational double-forces are evaluated.

In Fig. 12, the nodal material forces at the spatial mesh are plotted for a variation of the internal lengths l at the same (fixed) scale-transition parameter p as before. We observe that for zero internal length, the material force at the hole exhibits a distinct maximum at the lateral edges, while for increasing internal length, the material forces are more evenly distributed along the edge. The size of the material force vectors reflects the deformation along the free edges, particularly around the hole. Consequently, we may conclude that the additional stiffness imposed by the microstructure for larger internal length reduces the possible energy release at the defect.

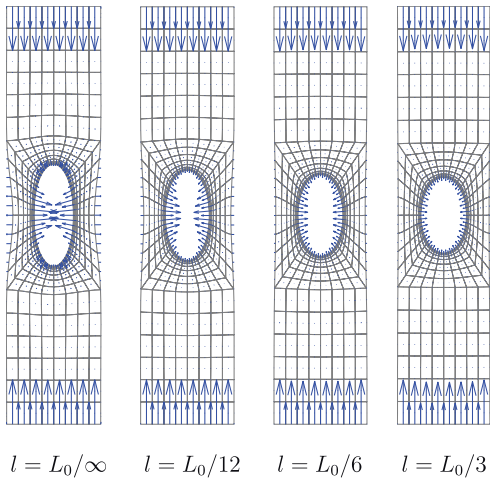

Fig. 12. Material forces $\mathfrak{F}_L$ on spatial mesh for variation of the internal length at $p = 20\,E$.

Now we consider the nodal configurational double-force $\bar{\mathfrak{m}}_J$, which is a non-symmetric tensor of second-order. First we display its modulus, $\|\bar{\mathfrak{m}}_J\|$, plotted continuously over the entire domain in Fig. 13. Generally it can be observed that the configurational double-force occurs in the interior of the domain, especially at the defect. For zero internal length, the double-force vanishes. This observation correlates with the fact that for this particular set of parameters the micromorphic continuum is very similar to the classical continuum due to the vanishing size of the microstructure being represented by the internal length l. Once a non-zero internal length is present, the nodal configurational double-force arises. But due to the more homogeneous deformation at large l, the distribution becomes more homogeneous and overall smaller.

To illustrate this quantity more characteristically, in Fig. 14 we display the results of the eigenvalue problem (confer Remark 5.1).

Remark 5.1 (*Eigenvalue problem*). For the non-symmetric tensor of second order, $\bar{\mathfrak{m}}_J$, both the left

$$\bar{\boldsymbol{a}}_J \cdot \bar{\mathfrak{m}}_J = \lambda_{aJ} \bar{\boldsymbol{a}}_J$$

and the right

$$\bar{\mathfrak{m}}_J \cdot \bar{\boldsymbol{b}}_J = \lambda_{bJ} \bar{\boldsymbol{b}}_J,$$

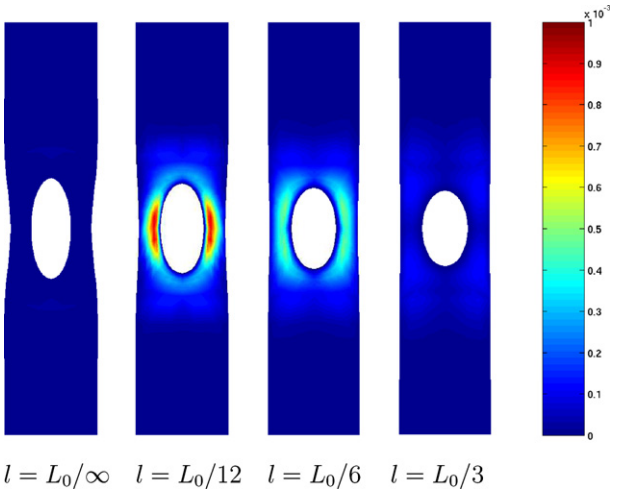

Fig. 13. Modulus of nodal configurational double-forces, $\|\bar{\mathfrak{m}}_J\|$, plotted continuously on spatial mesh for variation of the internal length at $p = 20\,E$.

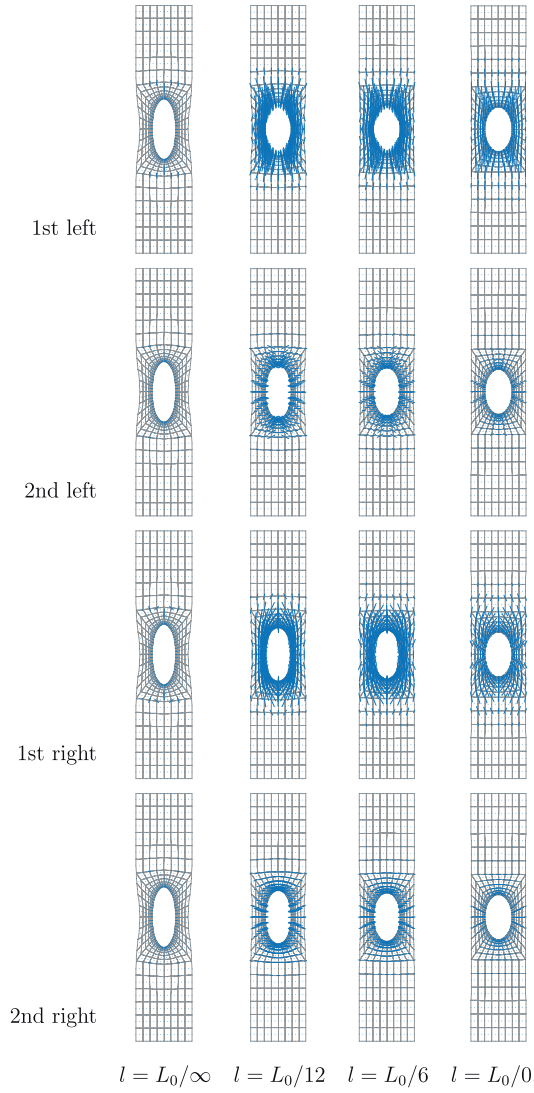

Fig. 14. Nodal configurational double-force $\bar{\mathfrak{m}}_J$: first versus second eigenvectors scaled by corresponding eigenvalues, plotted on spatial mesh for variation of internal length at scale-transition parameter $p = 20\,E$.

eigenvalue problem need to be considered. Herein $\bar{\boldsymbol{a}}_J$ denotes the left and $\bar{\boldsymbol{b}}_J$ the right eigenvector of $\bar{\mathfrak{m}}_J$, while the right and left eigenvalues are given by $\lambda_{aJ} = \lambda_{bJ}$.

Particularly, in Fig. 14 the first and the second left and right eigenvectors of the nodal configurational double-force at the finite element nodes are plotted, each one scaled by its corresponding eigenvalue. Here we notice a very distinct pattern: The first impression is that with increasing internal length the quantity decreases as already seen before in Fig. 13. Furthermore, we observe that the first left and the second right eigenvectors are oriented normal to each other, also the second left and the first right, which coincides with the eigenproblem theory. Especially for the first right eigenvectors, we notice that with increasing internal length, the arrows of significant size become less aligned at the hole. The first eigenvectors represent the "stronger" direction. Thus we conclude that the nodal configurational double-force, which is the microquantity being energetically conjugate to the microdeformation map of the material-motion problem, reflects a deflection of the loading from the edge of the hole to the remaining bulk aside.

5.2. Uniaxial loading of cracked specimen

As a second geometry, a rectangular specimen with a one-sided, non-propagating crack at half length under uniaxial quasi-static loading is examined. The crack, which experiences mode-I loading, is explicitly modelled by an additional edge in the finite-element mesh. For this boundary-value problem, first the internal length l and thereafter the penalty p is varied. Like in the previous example, the specimen is fixed at the bottom, and a constant displacement boundary condition is applied at the top nodes in longitudinal direction step-wise until a final elongation of $L_0/3$ is reached.

5.2.1. Results from the spatial-motion problem

First the influence of a variation of the internal length is studied at fixed scale-transition parameter, before the latter parameter is varied for fixed internal length.

For variation of the internal length l, the normal component of the Cauchy-type macrostress in loading direction at penalty parameter $p = 20\,E$ is plotted on the spatial

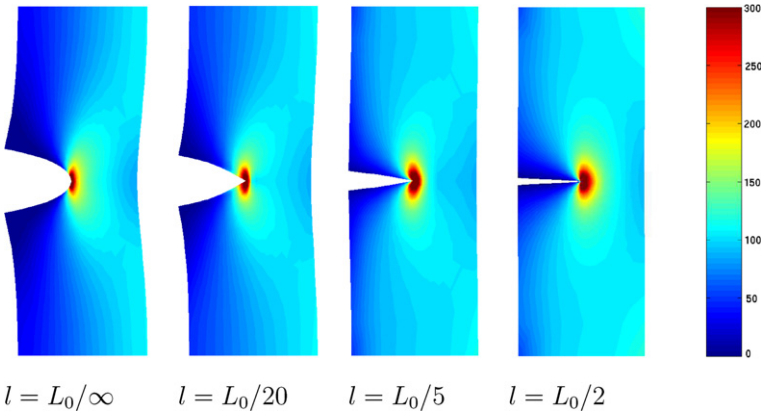

Fig. 15. Cauchy stress σ_{22} for a variation of the internal length at $p = 20\,E$.

configuration in Fig. 15. We observe that for increasing internal length, the crack opening becomes much smaller, which we can interpret as overall behaviour of the specimen becoming ascendingly stiff. For smaller l the regions within the specimen carrying none or minor load, are much larger. Contrarily, for a large internal length the stress is distributed over almost the entire specimen, and this distribution deflected strongly next to the crack.

Fig. 16 shows the modulus of the difference between macro and microdeformation from the scale-transition term $\|\bar{\boldsymbol{F}} - \boldsymbol{F}\|^2$ for varying internal length plotted on the spatial configuration at a penalty of $p = 20\,E$. For larger internal length, the region, in which this term is significant, increases, but remains narrowly aligned around the crack tip.

Further studies are made on the influence of the scale-transition parameter p. In Fig. 17, the normal Cauchy-type

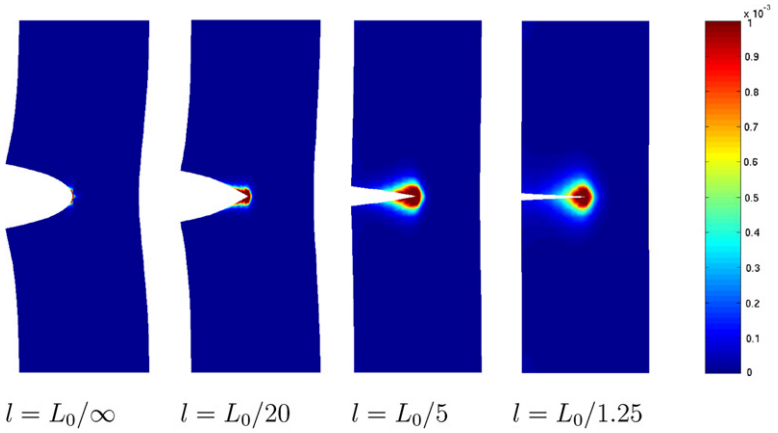

Fig. 16. Scale-transition measure $\|\bar{\boldsymbol{F}} - \boldsymbol{F}\|^2$ for variation of the internal length at $p = 20\,E$.

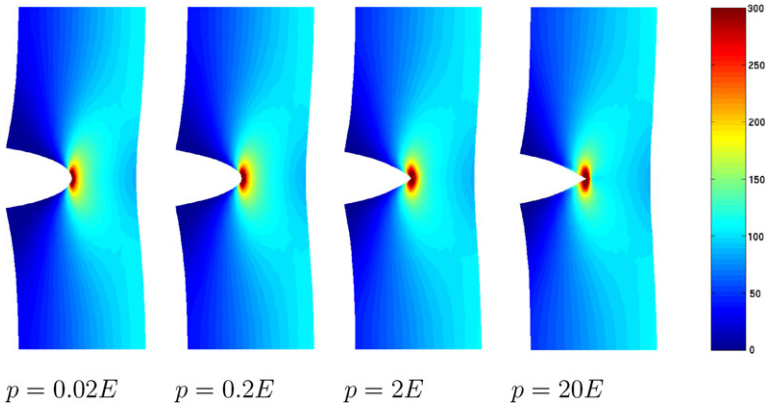

Fig. 17. Cauchy stress σ_{22} for variation of scale-transition parameter at $l = L_0/20$.

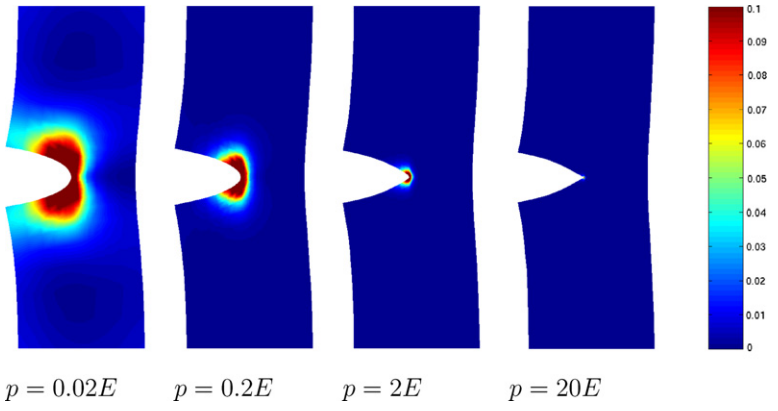

Fig. 18. Scale-transition measure $\|\bar{\boldsymbol{F}} - \boldsymbol{F}\|^2$ for variation of scale-transition parameter at $l = L_0/20$.

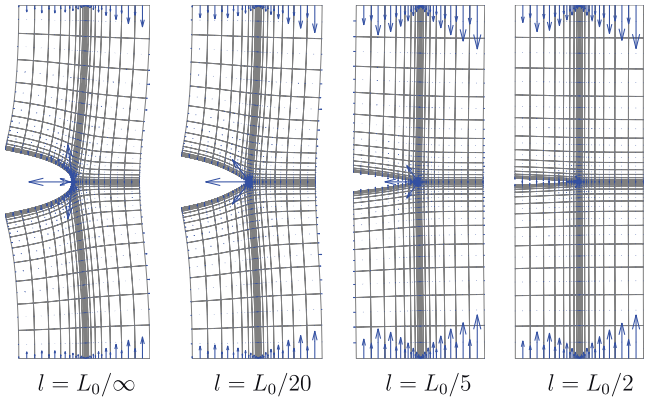

Fig. 19. Discrete material forces $\mathfrak{F}_L$ on spatial mesh at variation of the internal length at $p = 20\,E$.

macrostress component in longitudinal direction, σ_{22}, is plotted on the spatial mesh and compared for different scale-transition parameters p. The spatial mesh changes in such manner that, for increasing p, the shape of the crack tip changes from rounded to sharp. The influence of p on the stress σ_{22} is not as strong as that of the internal length. Mainly the field at the crack tip changes its shape from a "0" towards that of an "8".

Now the influence of the parameter p on the kinematic measurement from the scale-transition term, $\|\bar{\boldsymbol{F}} - \boldsymbol{F}\|^2$, is investigated. From the plot of this field in Fig. 18, we may perceive that only a rather high scale-transition parameter leads to a successful penalisation of the quantity, since then the macrotangent and the microdeformation map, $\boldsymbol{F}$ and $\bar{\boldsymbol{F}}$ approach each other. Only around the crack tip, an occurrence can still be recognised for a penalisation being sufficient elsewhere over the domain. This behaviour is characteristic for the formulation as explained in the sequel: For small values of p the microcontinuum deforms more independently as characteristic for microcontinuum theory. Opposed to that, the formulation approaches a gradient continuum for larger values of p.

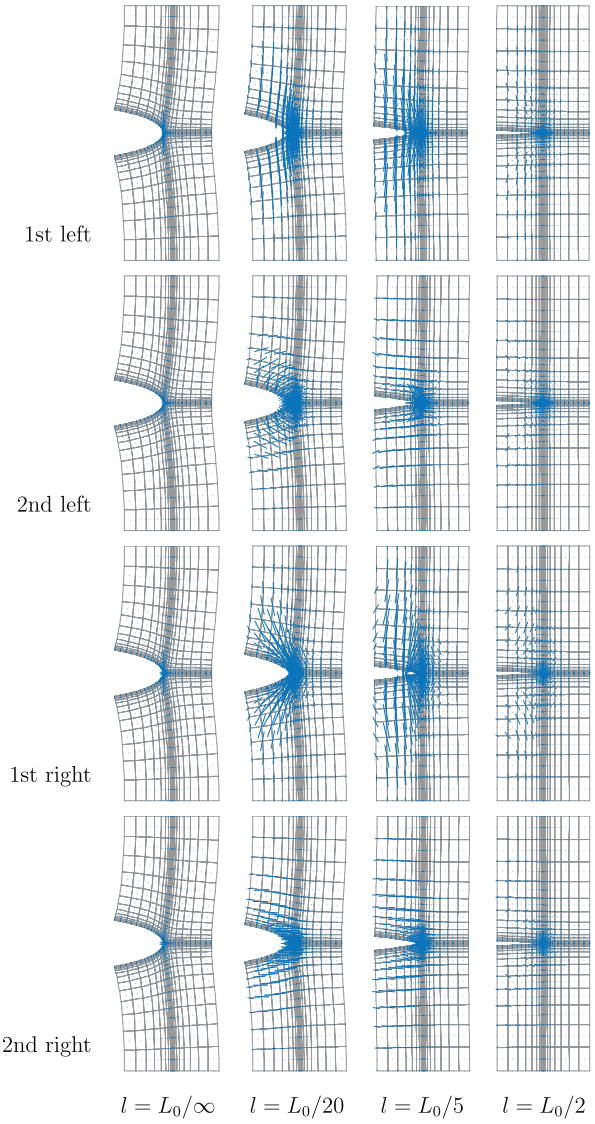

Fig. 21. Nodal configurational double-force $\bar{\mathfrak{m}}_I$: eigenvectors scaled by corresponding eigenvalues, plotted on spatial mesh for variation of internal length at scale-transition parameter $p = 20\,E$.

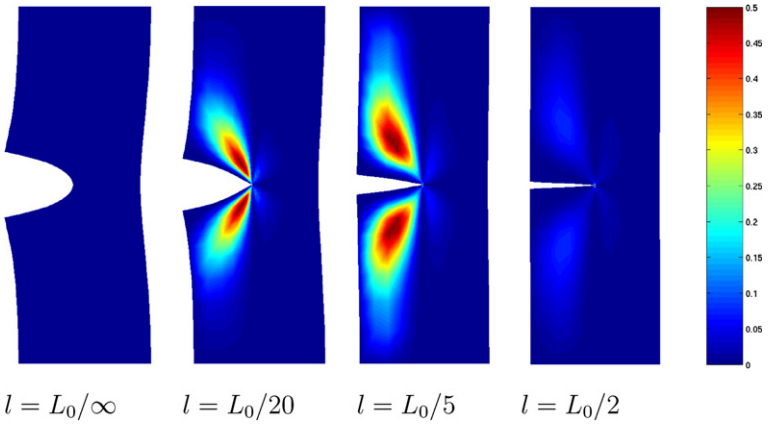

Fig. 20. Modulus of nodal configurational double-force, $\|\bar{\mathfrak{m}}_I\|$, plotted continuously on spatial mesh for variation of internal length at scale-transition parameter $p = 20\,E$.

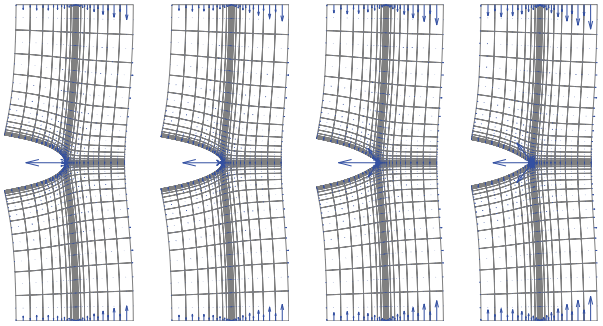

Fig. 22. Discrete material forces $\mathfrak{F}_L$ on spatial mesh variation of scale-transition parameter at $l = L_0/20$.

This goes along with locally compatible deformations, which are here imposed by the penalising scale-transition term.

5.2.2. Results from the material-motion problem

For the cracked specimen, the material force method is applied. First the nodal material forces resulting from the balance of macromomentum are plotted for a variation of the internal length and of the scale-transition parameter, before the nodal configurational double-forces are presented for the same sets of parameters.

In Fig. 19 the discrete nodal material forces $\mathfrak{F}_L$ are plotted for different values of the internal length. The material forces occur along all edges, especially on the fixed boundaries at the upper and lower at end of the specimen and at the crack tip. Particularly, there is one large lateral material force located at the crack tip and directed opposite to the direction into which the crack would propagate. We observe that with increasing internal length, the overall deformation is more homogeneous and the major material force vector at the crack tip decreases. At the same time, those material force vectors representing the boundary reaction forces become larger. This can be attributed to

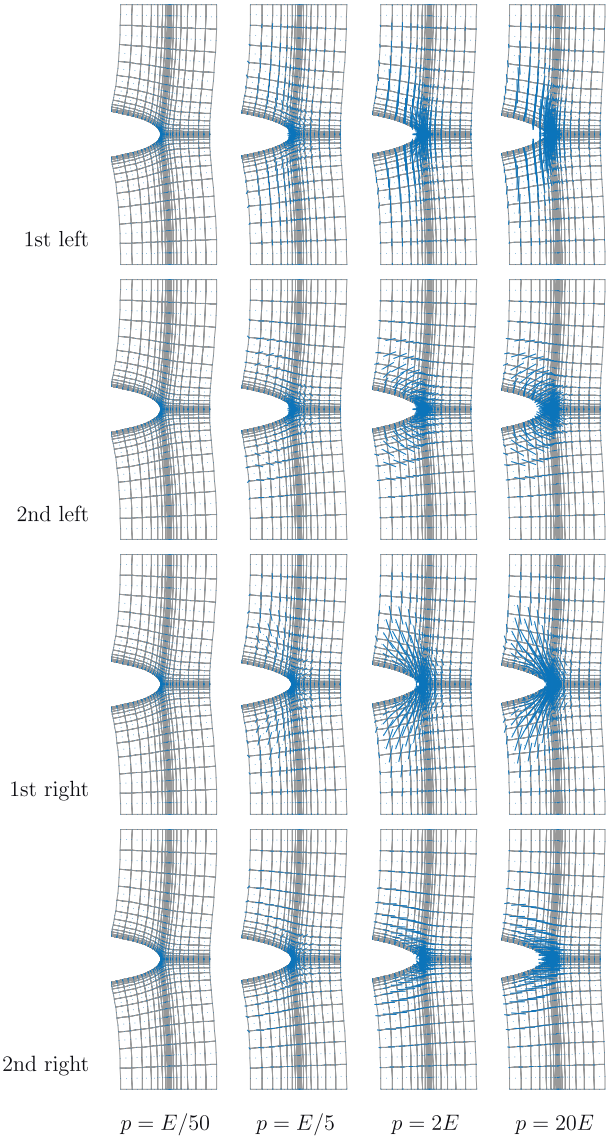

Fig. 24. Nodal configurational double-force $\bar{\mathfrak{m}}_J$: eigenvectors scaled by corresponding eigenvalues, plotted on spatial mesh for variation of scale-transition parameter at internal length at $l = L_0/20$.

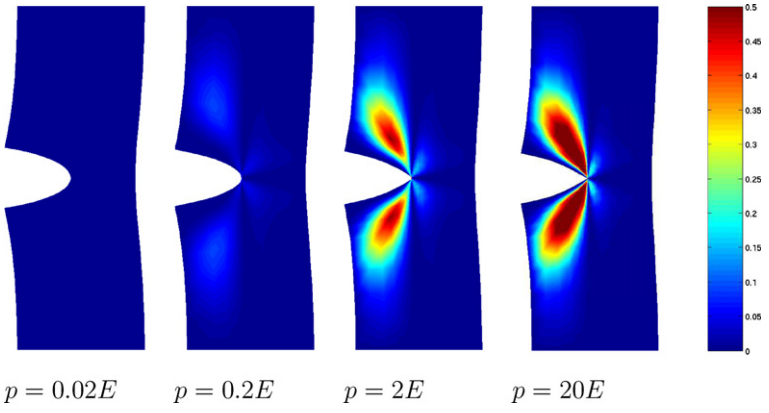

Fig. 23. Modulus of nodal configurational double-force, $\|\bar{\mathfrak{m}}_J\|$, plotted continuously on the spatial mesh for a variation of scale-transition parameter at $l = L_0/20$.

the fact that the parameter increases the stiffness: for the same displacement, the stiffer specimen will exhibit higher stresses and thus bear a larger load.

In the sequel, we regard the results for the nodal configurational double force of the microscale, $\bar{\mathfrak{m}}_J$. In this context, Fig. 20 shows its modulus, $\|\bar{\mathfrak{m}}_J\|$, again plotted continuously over the mesh. Here we observe the same phenomenon as for the previous specimen: For zero internal length the modulus is zero everywhere, while the quantity has the biggest values for the smallest non-zero internal length and the occurrence decreases with growing internal length. This behaviour is also reflected in the illustration of the eigenvalue problem in Fig. 21. Besides this, we moreover observe that, with increasing internal length, the orientation of the eigenvectors changes. This could be attributed to a switch in the order of the corresponding eigenvalues, which consequently determine the direction of the eigenvectors.

We now look at the influence of the scale-transition parameter p on the material forces, see Fig. 22. Despite the aforementioned change in the crack shape, for larger p the material force distribution experiences no significant sensibility to the scale-transition parameter. Only the material forces at the supported edge become slightly larger, which indicates a slightly stiffer behaviour of the specimen for increasing p.

Contrary to this, the norm of the nodal configurational double-force of the microscale, $\|\bar{\mathfrak{m}}_J\|$, plotted in Fig. 23, occurs increasingly stronger for increasing scale-transition parameter p. This strong influence of p on the quantity of the nodal configurational double-force also becomes obvious in Fig. 21. This time, there is no significant change in direction of the eigenvectors. We may conclude that, as the formulation approaches a second-order gradient continuum, the micro nodal configurational double-forces grow (see Fig. 24).

6. Summary and conclusion

In the present contribution, we have introduced a micromorphic continuum formulation which is characterised by the additional consideration of a microstructure attached at each continuum point. Thus we have introduced additional kinematic quantities, to account for both the macro and the microscale, and with these derived the balance relations. The theory has completely been introduced in terms of two perspectives: the spatial- and the material-motion problem. Their duality was especially pointed out by presenting the relations of the kinematic quantities, the stress quantities and the balance relations. Furthermore, we have presented a hyperelastic constitutive relation, which accounts for both the macro and the microscale, and additionally couples both by a so-called scale- transition term. With this complete framework at hand, a finite-element approximation scheme has been presented, which allows the solution of boundary-value problems being coupled with respect to macro and microquantities. In the sense of the material-motion problem, we have applied the material force method to the present theory. Here, besides nodal material forces of the macroscale, which conform to those known from local continua, we have derived an additional quantity for the microscale, the nodal configurational double forces. These quantities will prove useful when considering defect mechanics for micromorphic or related generalised continua.

We have completed our contribution by numerical examples. Within these, we have solved the spatial-motion problem and furthermore evaluated the presented quantities from the micromorphic material force method. On the one hand, we have been able show that our theory reflects the typical features, such as non-symmetric stress etc. On the other hand, we obtained results of the material force method that will be used when focusing on defect mechanics for generalised continua.

Acknowledgements

We gratefully acknowledge financial support by the German Science Foundation DFG within the International Research Training Group 1131 "Visualization of Large and Unstructured Data Sets – Applications in Geospatial Planning, Modeling, and Engineering".

References

[1] E. Amanatidou, A. Aravas, Mixed finite element formulations of strain-gradient elasticity problems, Comput. Methods Appl. Mech. Engrg. 191 (2002) 1723–1751.
[2] E. Cosserat, F. Cosserat, Théorie des Corps Déformables, Herman et fils, Paris, 1909.
[3] E. Diegele, R. Elsäßer, C. Tsakmakis, Linear micropolar elastic crack-tip fields under mixed mode loading conditions, Int. J. Fract. 129 (2004) 309–339.
[4] W. Ehlers, W. Volk, On theoretical and numerical methods in the theory of porous media based on polar and non-polar elasto-plastic solid materials, Int. J. Solid Struct. 35 (1998) 4597–4617.
[5] M. Epstein, G.A. Maugin, The energy–momentum tensor and material uniformity in finite elasticity, Acta Mech. 83 (1990) 127–133.
[6] A.C. Eringen, Mechanics of micromorphic materials, in: H. Görtler (Ed.), Proc. 11th Int. Congress of Appl. Mech., Springer-Verlag, New York, 1964, pp. 131–138.
[7] A.C. Eringen, Mechanics of micromorphic continua, in: E. Kröner, (Ed.), Mechanics of Generalized Continua, Freudenstadt/Stuttgart, 28 August–2 September 1967–1968. IUTAM Symposium, Springer.
[8] A.C. Eringen, Microcontinuum Field Theories: I. Foundations and Solids, Springer, New York, 1999.
[9] P. Grammenoudis, C. Tsakmakis, Hardening rules for finite deformation micropolar plasticity: Restrictions imposed by the second law of thermodynamics and the postulate of Il'Iushin, Continuum Mech. Therm. 13 (2001) 325–363.
[10] M.E. Gurtin, Configurational forces as basic concepts of continuum physics, Appl. Math. Sci., vol. 137, Springer, 2000.
[11] N. Kirchner, P. Steinmann, A unifying treatise on variational principles for gradient and micro-morphic continua, Philos. Magn. 85 (2005) 3875–3895.
[12] N. Kirchner, P. Steinmann, On the material setting of gradient hyperelasticity, Math. Mech. Solid, in press, doi:10.1177/0021998306067073.
[13] W.T. Koiter, Couple-stresses in the theory of elasticity, I and II, Proc. Roy. Netherlands Acad. Sci. (B) 67 (1964) 17–44.

[14] V.G. Kouznetsova, Computational homogenization for the multiscale analysis of multi-phase materials, Ph.D. thesis. Technische Universiteit Eindhoven, 2002.
[15] V.G. Kouznetsova, M.G.D. Geers, W.A.M. Brekelmans, Multi-scale constitutive modelling of heterogeneous materials with a gradient-enhanced computational homogenization scheme, Int. J. Numer. Methods Engrg. 54 (2002) 1235–1260.
[16] V.G. Kouznetsova, M.G.D. Geers, W.A.M. Brekelmans, Multi-scale second-order computational homogenization of multi-phase materials: a nested finite element solution strategy, Comput. Methods Appl. Mech. Engrg. 193 (2004) 5525–5550.
[17] E. Kuhl, H. Askes, P. Steinmann, An ALE formulation based on spatial and material settings of continuum mechanics – Part 1: Generic hyperelastic formulation, Comput. Methods Appl. Mech. Engrg. 193 (2004) 4207–4222.
[18] T. Liebe, R. Denzer, P. Steinmann, Application of the material force method to isotropic continuum damage, Comput. Mech. 30 (2003) 171–184.
[19] G.A. Maugin, Material Inhomogeneities in Elasticity, Chapman and Hall/CRC, 1993.
[20] G.A. Maugin, Material forces: Concepts and applications, Appl. Mech. Rev. 48 (1995) 213–245.
[21] G.A. Maugin, P. Steinmann, Mechanics of material forces, Adv. Mech. Math., vol. 11, Springer, 2005.
[22] R.D. Mindlin, H.F. Tiersten, Effects of couple-stress in linear elasticity, Arch. Rat. Mech. Anal. 11 (1962) 415–448.
[23] R. Mueller, G.A. Maugin, On material forces and finite element discretizations, Comput. Mech. 29 (2002) 52–60.
[24] J.Y. Shu, C.Y. Barlow, Strain gradient effects on microscopic strain field in a metal matrix composite, Int. J. Plast. 16 (2000) 563–591.
[25] J.Y. Shu, W.E. King, N.E. Fleck, Finite elements for materials with strain gradient effects, Int. J. Numer. Methods Engrg. 44 (1999) 373–391.
[26] P. Steinmann, A micropolar theory of finite deformation and finite rotation multiplicative elastoplasticity, Int. J. Solid Struct. 31 (1994) 1063–1084.
[27] P. Steinmann, Application of material forces to hyperelastostatic fracture mechanics. I. Continuum mechanical setting, Int. J. Solid Struct. 37 (2000) 7371–7391.
[28] P. Steinmann, On spatial and material settings of thermo-hyperelastodynamics, J. Elastic. 66 (2002) 109–157.
[29] P. Steinmann, E. Stein, A unifying treatise of variational principles for two types of micropolar continua, Acta Mech. 121 (1997) 215–232.
[30] P. Steinmann, D. Ackermann, F.J. Barth, Application of material forces to hyperelastostatic fracture mechanics. II. Computational setting, Int. J. Solid Struct. 38 (2001) 5509–5526.
[31] R.A. Toupin, Elastic materials with couple-stress, Arch. Rat. Mech. Anal. 17 (1962) 85–112.
[32] R.A. Toupin, Theory of elasticity with couple-stress, Arch. Rat. Mech. Anal. 11 (1964) 385–414.